RJC

RASĀYAN ***J. Chem.***
Vol. 16 | No. 4 |2126-2153| October - December | 2023
ISSN: 0974-1496 | e-ISSN: 0976-0083 | CODEN: RJCABP
http://www.rasayanjournal.com
http://www.rasayanjournal.co.in

CYTOTOXIC, ANTIMICROBIAL, AND ANTIOXIDANT ACTIVITIES OF BIMETALLIC LANTHANUM AND COBALT COMPLEXES

K. R. Swathi[1], M. N. Somashekar[2] and P. R. Chetana[3,✉]

[1]Department of Chemistry, Jnana Bharathi Campus, Bangalore University, Bengaluru, Karnataka-560056, India

[2]Department of Chemistry, S. S. Margol Degree College of Arts, Science, and Commerce, Shahabad, Kalaburagi District, Karnataka-585228, India

[3]Department of Chemistry, Central College Campus, Bengaluru City University, Bengaluru, Karnataka-560001, India

✉Corresponding Author: pr.chetana@gmail.com

ABSTRACT

We have synthesized new mono nuclear Cobalt(II) complex and hetero binuclear lanthanide(II) and cobalt(II) complexes with general formulation $[Co(L_1)_2]X$ (2), $[Co(L_1)M(L_2)_2]X_2$ (3) and $[Co(L_1)M(L_2)_2(NO_3)]X_2$ (4) respectively where, L_1 is N,N-bis[2-(dimethylamino)ethyl]oxalamide (1), L_2 is *N*,*N*-donor heterocyclic base 1,10-phenanthroline, M is copper(II)/lanthanide(II) and X is ClO_4^-/NO_3^-. These complexes were characterized by CHNS elemental analysis and IR, NMR, and ESI-MS spectral data. The cytotoxic studies on selected cell lines to evaluate half maximal inhibitory concentration (IC_{50}) value and were tested for apoptotic phase and cell cycle arrest for HeLa and HT-29 cell lines using propidium iodide and annexin V fluorescent dyes through flow cytometry technique. Antimicrobial and Antifungal activities were tested on selected bacterial and fungal strains respectively. Antioxidant activity was carried out by DPPH free radical scavenging, nitric oxide, and superoxide dismutase assay. DNA binding studies were investigated by electronic absorption and gel electrophoresis methods to evaluate their binding efficiency.

Keywords: Co (II)/La(II) Complexes, Cytotoxic Studies, Cell Cycle, Apoptosis, Antioxidant, Antimicrobial Activity.

RASĀYAN *J. Chem.*, Vol. 16, No. 4, 2023

INTRODUCTION

The development of ligands and the choice of metal ions in the context of DNA interactions with metal complexes have thus been the subject of extensive research. It is well known that metal ions in complexes with other metals can boost up the action of medications and enhance the potency of organic ligands. Therefore, it is believed that a key step in developing a highly effective metal-based drug is choosing the appropriate metal and designing the appropriate ligand.[1-5] As a result of Sigman et al discovery's that 1,10-phenanthroline (phen) coordinated to copper ion can cleave DNA[6] were inspired to design and synthesize new bimetallic complexes with asymmetric N,N′-bis(substituted)-oxamides as bridging ligands in assess as well as to comprehend the effect of various asymmetric N,N′-bis(substituted)oxamide bridging ligands on structure, we studied the DNA-binding characteristics and antitumor activity associated with these types of complexes.[7]

EXPERIMENTAL

Materials and Methods

All the chemicals used were of AR quality and were utilized precisely as directed. To assess the antimicrobial efficacy of synthesized mono and bimetal complexes, selected bacterial and fungal strains from the ATCC were used. Cancer cell lines were procured from the ATCC and analyzed on a Tecan Plate reader to evaluate the antineoplastic activity of metal complexes. FACS Caliber (BD Biosciences, San Jose, CA) using propidium iodide and RPMI medium (Roswell Park Memorial Institute Medium, which includes biotin, vitamin B_{12}, and para-aminobenzoic acid (PABA); RNase A, which was purchased from Boehringer Mannhein GmbH; 5 mg/ml stock concentration, 0.05mg/ml working solution

http://doi.org/10.31788/RJC.2023.1648501

concentration), flow cytometry was employed to record fluorescence during cell cycle and apoptosis experiments. Using a Bruker Ascend 800 MHz NMR instrument, the proton NMR spectra were collected. Using potassium bromide pellets the IR spectra of the synthesized compounds were recorded with a Shimadzu spectrophotometer and a Perkin Lambda 35 spectrophotometer was used to document the FTIR spectra. ESI and APCI probe-equipped Schimadzu-LCMS instrument was used to document mass spectra. UV-visible spectra were produced using a Systronics 2206, a PC-based dual-beam UV spectrophotometer. At the Institution of Excellence in Mysore, elemental studies were carried out using a Bruker Euro Ea elemental analyzer. The molar conductance of the complexes was assessed using a Control Dynamics APX185E conductivity probe with a dip-type cell using reagent grade 0.1M KCl for calibration. The melting points were investigated using manual equipment.

Synthesis of N^1, N^2-bis(2-(dimethylamino)ethyl)oxalamide; dmedox (1)

According to Scheme-1**,** in an ice bath, drop by drop, homogeneous ethanol and diethyl oxalate solution (499 mL, 0.1 M, 20 mL) were poured with continual stirring to N^1, N^1-dimethylethane-1,2-diamine (271 µL, 0.2 M, 20 mL), which had been cooled to 2-3° C. After the completion of addition, approximately five hours were spent heating the reaction mixture in a water condenser at 60 °C at constant stirring. The reaction mixture obtained produced a white-colored precipitate after 8 days of gradual evaporation at room temperature. Warm ethanol-water (1:1 v/v) was used to wash the resulting white solid. Recrystallization from ethanol was performed in hot conditions and dried over P_2O_5 and 88.4 percent yield (1) was obtained.

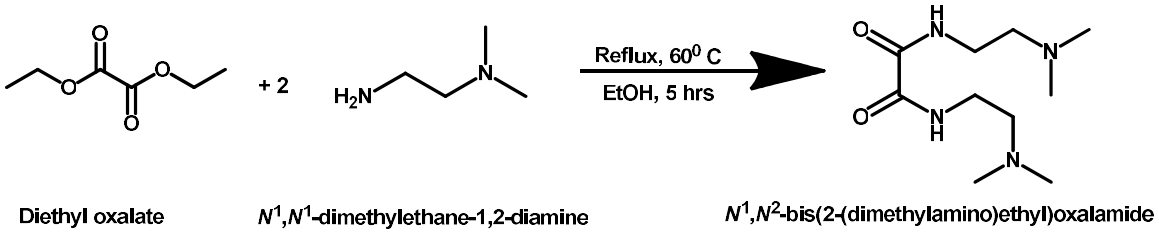

Scheme-1: Propound Synthetic Path of N^1, N^2-bis(2-(dimethylamino)ethyl)oxalamide Ligand 1

Analytical calculation percentages for $C_{10}H_{22}N_4O_2$; (5): C, 52.15; H, 9.63; N, 24.33. Found C, 52.16; H, 9.68; N, 24.34. ^{1}H-NMR (400 MHz, DMSO-d_6, ppm): δ = 1.02 – 3.49(s, 12H), 2.51 – 3.59(t, 4H), 4.64 – 4.67(d, 4H). FT-IR (KBr disc, cm^{-1}): ν = 1584**,** (C=O), 3548 (N-H). λ_{max} (10^{-3} M, DMF/Tris-HCl): 22 nm (ε = 13,066 M^{-1} cm^{-1}). ESI-MS (m/z): 230.9 [M^+]. yield: 88.4%. M.P: 89-90 ^{0}C.

Synthesis of {µ-trans- N^1, N^2-bis(2-(dimethylamino)ethyl)oxamidato}(cobalt(II) tetraoxidochlorate); [Co(dmedox)$_2$] (ClO_4^-) (2)

As given in Scheme-2, drop by drop ethanolic solution of 0.1 M dmedox (1) was added to the $CoCl_2.6H_2O$ (0.1 M, 0.237 g, 10 mL) that had been agitated for three hours. The resultant purple-colored particles were removed through filtration, carefully cleansed with hot ethanol and diethyl ether before being dried at low pressure over P_2O_5.[8] Recrystallization from ethanol was performed in hot condition and 78.2 percent yield was obtained.

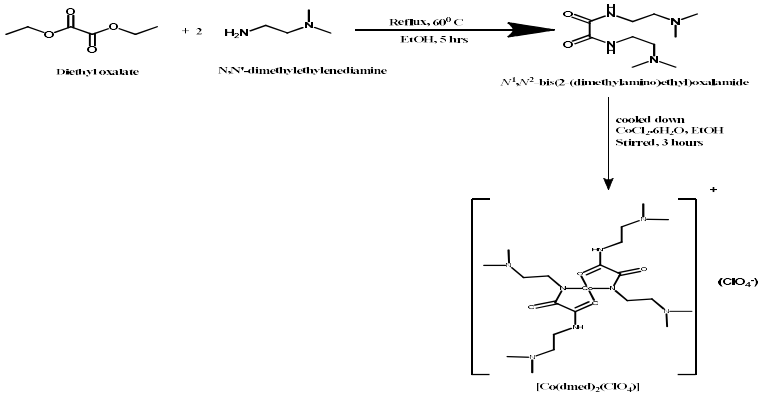

Scheme-2: Propound Synthetic Path for Complex 2

Analytical calculation percentages for $C_{20}H_{42}ClCoN_8O_8$; (6): C, 38.93; H, 6.86; N, 18.16. Found C, 38.86; H, 6.84; N, 18.17. ^{1}H-NMR (400 MHz, DMSO-d_6, ppm): δ = 1.25 – 3.12(s, 12H), 3.26 – 3.30(t, 8H), 8.32 – 8.48(m, 2H). FT-IR (KBr disc, cm^{-1}): ν =1650 (C=O), 3297 (N-H). λ_{max} (10^{-3} M, DMF/Tris-HCl): 22 nm (ε = 13,066 M^{-1} cm^{-1}). ESI-MS (m/z): 616.2 [M^+] where M = $[Co(dmedox)_2]^{2+}$. Λ_M (DMF, S cm^2 M^{-1}): 80.25. yield: 78.2%. M.P: 112-114 ^{0}C.

Synthesis of {N,N′-bis(2-(dimethylamino)ethyl)oxamidato}(1,10-phenanthroline) cobalt(II)copper(II)dinitrate; [Co(dmedox)Cu(phen)$_2$] (NO$_3$)$_2$ (3)

dmedox (0.1 mM, 0.460 g, 20 mL) and triethyl amine (0.2 mM, 278 L, 10 mL) solutions were sequentially added to a $Co(NO_3)_2.6H_2O$ (0.095 mM, 0.276 g, 10 mL) and triethyl amine (0.2 mM, 278 L, 10 mL) solution. The obtained mixture was then swirled at 26-27 ^{0}C for about 30 minutes until it was limpid. After that, contaminants were removed from the reaction mixture by filtering. Under N_2, methanolic solutions of $Cu(NO_3)_2.3H_2O$ (0.1 mM, 0.241 g, 10 mL) and heterocyclic base 1,10-phenanthroline (0.2 mM, 0.360 g, 10 mL) to the aforementioned reaction mixture were added drop by drop. A 9-hour reflux process was then performed on the reaction mixture (Scheme-3), the precipitate that resulted was removed using warm methanol and diethyl ether under reduced pressure, and it was thoroughly cleaned before being dried over P_2O_5.[8] For recrystallization, a 1:3 mixture of DMF and methanol was utilized.

Analytical calculation percentages for $C_{34}H_{36}CoCuN_{10}O_6$; (7): C, 48.89; H, 4.34; N, 16.77. Found, C, 48.80; H, 4.68; N, 16.76. ^{1}H-NMR (400 MHz, DMSO-d_6, ppm): δ = 1.4 – 2.0(s, 12H), 3.1– 3.2(t, 2H), 7.3 – 8.6(m, 8H). FT-IR (KBr disc, cm^{-1}): ν = 1601(C=O), 1382 (NO_3^- ionic,), 558 (M-O), 429 (M-N), ESI-MS (m/z): 258.9 [M +2K]$^{2+}$. λ_{max} Water/DMF (5%): 217 nm (ε = 16,330 M^{-1} cm^{-1}), 241 nm (ε = 14,566 M^{-1} cm^{-1}) and 266 nm (ε = 25,000 M^{-1} cm^{-1}). ESI-MS (m/z): 356.6 [M+H-2(NO_3^-)] $^+$ where M=$[Co(dmedox)Cu(phen)_2]^{2+}$. Λ_M (DMF, S cm^2 M^{-1}): 137.69. yield: 68.5%. M.P: 122-124 ^{0}C.

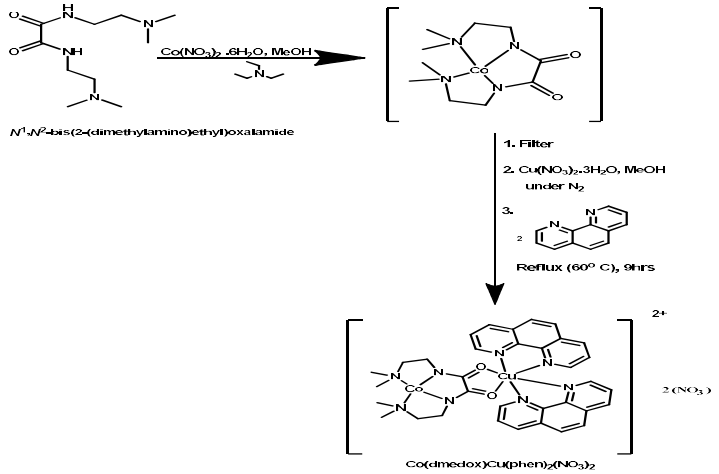

Scheme-3: Propound Synthetic Path for Complex 3

Synthesis of Trioxidonitrate{N, N′--bis(2-(dimethylamino)ethyl)oxamidato} (1,10-phenanthroline)Cobalt(II)Lanthanum(III)dinitrate;[Co(dmedox)La(phen)$_2$ (NO$_3$)] (NO$_3$)$_2$ (4)

$Cu(NO_3)_2$.$3H_2O$ (0.095 mM, 0.229 g, 10 mL) and triethyl amine (0.2 mM, 278 L, 10 mL) methanolic solutions were successively added to a dmedox (0.1 mM, 0.515 g, 20 mL) solution that was agitated in methanol. The obtained mixture was then swirled at 26 -27 ^{0}C for about 30 minutes until it was limpid. After that, contaminants were removed from the reaction mixture by filtering. Methanolic solutions of $Co(NO_3)_2.6H_2O$ (0.1 mM, 0.460 g, 20 mL) and 1,10-phenanthroline (0.2 mM, 0.360 g, 10 mL) were added dropwise under N_2 to this reaction mixture. The obtained mixture was next heated constantly at 60 ^{0}C using a reflux condenser for nine hours (Scheme-4), the precipitate that resulted was then filtered out and it was thoroughly cleansed with warm methanol followed by diethyl ether, under decreased pressure the product was dried over P_2O_5.[8] For recrystallization, a 1:3 mixture of DMF and methanol was utilized.

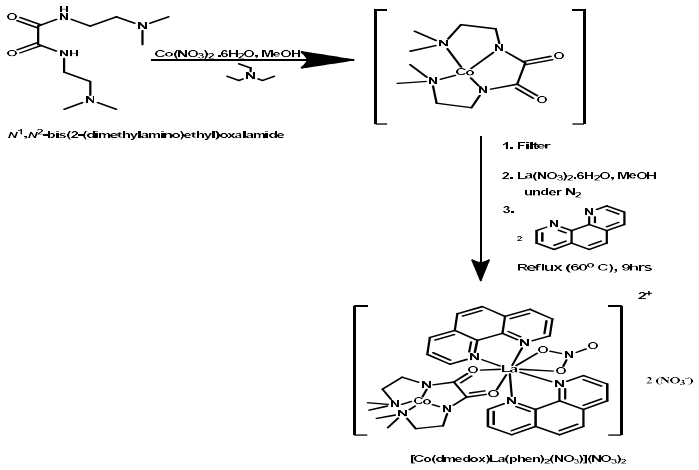

Scheme-4: Propound Synthetic Path for Complex 4

Analytical calculation percentages for $C_{34}H_{36}CoLaN_{11}O_{11}$; (8): C, 41.99; H, 3.73; N, 15.84. Found, C, 41.96; H, 3.75; N, 15.67. ^{1}H-NMR (400 MHz, DMSO-d_6, ppm): δ = 1.5 – 1.6(s, 12H), 2.4 – 2.5(t, 2H), 7.6 – 8.9(m, 8H). FT-IR (KBr disc, cm^{-1}): 1607(C=O), 1352 (NO_3^- ionic,), 561 (M-O), 410 (M-N). λ_{max} Water/DMF (5%): 211 nm (ε = 21695.3 M^{-1} cm^{-1}), 340 nm (ε = 34959.28 M^{-1} cm^{-1}) and 377.5 nm (ε = 38815.09 M^{-1} cm^{-1}). ESI-MS (m/z): 425.3 $[M+H-2(NO_3^-)]^+$ where M = $[Co(dmedox)La(phen)_2(NO_3)]^{2+}$. Λ_M (DMF, S cm^2 M^{-1}): 150.32. yield: 72.9%. M.P: 127-129 ^{0}C.

DNA Binding Studies

Investigations of Binding Efficacy of DNA by UV-Visible Absorption Technique

Using Calf thymus DNA, electronic absorption tests were conducted to test the DNA binding ability of 2, 3, and 4 complexes. The concentration of Calf thymus DNA was increased by 2.5 μM aliquots up to 10 μM during the experiments. To obliterate absorption caused by free CT-DNA, in the reference compartment, an equimolar amount of CT-DNA was mixed with a pure buffer solution to attribute spectra with metal complexes. The comparatively small shift in absorption intensity in response to DNA concentration was used to construct titration curves. The intrinsic binding constant was computed using titration curve analysis (K_b). The linear fit curve was plotted in Origin to assess the binding constant of metal complexes (version 6.1). By measuring UV-visible absorbance and recording incremental DNA addition by following equation (a), the binding constant of mono and bimetal complexes are calculated.[9]

$$[DNA]/(\varepsilon_a - \varepsilon_f) = [DNA]/(\varepsilon_b - \varepsilon_f)+1+/K_b(\varepsilon_b - \varepsilon_f)(a)$$

In the aforementioned equation, the extinction coefficients ε_a (for every additament of CT-DNA to the metal complex), ε_f (the complex without DNA; as determined by Beer's law from the calibration curve of the relevant metal complex), and ε_b (the complex when fully bound to DNA)

DNA Binding Studies by Gel Electrophoresis

Deoxyribonucleic Acid Binding Studies by Gel Electrophoresis Method

The complexation coherence of a DNA mixture was evaluated with the aid of gel electrophoresis and EtBr intercalation appraisal. Following an hour of incubation at room temperature, the prepared mixtures were infused into the gel at a concentration of 100 ng/well using gel-loading TAE buffer. Thereafter, 45 minutes of electrophoresis in 1 TAE buffer at 5 Vcm^{-1} were carried out. UV Trans illumination on the Chemi Doc Bio-rad was used to see how free DNA migrated on the gel. Using naked DNA bands as a standard, the amount of free DNA was measured, and band densities were calculated using the Image J1.50c program. The following expression was used to calculate the complexation coherence:

Complexation coherence (%) = (BD $_{Std}$ DNA − BD sample) × 100/BD$_{Std}$ DNA

Where BD_{std} DNA and BD sample stand for band densities with standard (free DNA or unbound DNA) and band densities of parent ligand dmpdox (1) and its corresponding metal complexes 2, 3 and 4, where band intensity gives the abundance of CT-DNA present after complexation with metal complexes.[10,11]

Free Radical Scavenging Activities of Metal Complexes

DPPH Radical Scavenging

Antioxidants convert purple-colored DPPH into the colorless molecule 1,1-diphenyl-2-picryl hydrazine, which is measured at an absorbance of 590 nm. DPPH scavenging for the ligand 1 and its mononuclear and binuclear complexes 2, 3, and 4 were found by amending the reported technique.[12] One milligram of prototype samples was mixed to create stock solutions for testing. Different test solution concentration was taken in a 96-well plate by twofold dilution and volumes were made up to 240 µL using HPLC grade methanol and 80 µL of DPPH was added to each well since DPPH is photosensitizer, an immediate 15-minute incubation in the dark at 25°C was performed on the reaction mixture. A blank solution without the test sample was carried out along with standard quercetin. Both the standard and blank solution wells were prepared using the same protocol as of test samples. Then, using a semi-autoanalyzer, absorbance was determined at 590 nm. Comparative studies of the metal complexes and the antioxidant quercetin were conducted. IC_{50} values and percent inhibition are calculated using nonlinear regression analysis, which is done for various test sample concentrations and reference samples. Percent of impediment was recorded for reference and different sample concentrations by nonlinear regression analysis by making use of Graph Pad Prism software version 6.0. The IC_{50} value is not calculated for samples that have inhibition levels below 50%. By contrasting the sample's IC_{50} value with the standard, the sample's relative DPPH scavenging activity was assessed. The relative activity will be lower about the standard if the IC_{50} value is higher, and vice versa.

Nitric Oxide Scavenging Assay

By modifying the previously published procedure,[15] the nitric oxide scavenging assay for ligand 1 and its mononuclear and binuclear complexes 2, 3, and 4 were determined. The diazotization reaction is the basis for the nitric oxide assay. In an acidic environment (phosphoric acid), sulfanilamide and N-1-napthylethylenediamine can identify NO_2 in cellular matrices like a serum, plasma, etc., and stock solutions for test samples were made by dissolving one milligram of the test substances in one milliliter of DMSO. 1 mL of a 1 mM nitrite standard (curcumin) was prepared in the pH 7.0 phosphate saline buffer (8 g of NaCl, 1.21g of K_2HPO_4, and 0.34g of KH_2PO_4 in 1000 mL distilled water.) For the experimental samples, 50 µL of the stock solution (160, 80, 40, 20, 100 µM) and standard (1000, 500, 250, 125, 6.25, and 31.3 µM) were added to the 96-well plate by twofold dilution concentration using a multichannel pipette. Buffer was added to the last set of wells with no test sample solutions. Each well's final volume was 50 µL and the nitrite concentration range was 0-1000 mM then 50 µL of Griess reagent (1g sulfanilamide solubilized in 5% H_3PO_4 solution in de-ionized water and 10 mg of 0.1% N – naphthyl ethylene diamine solubilized in 10 mL de-ionized water, was mixed in 1:1 ratio just before using the reagent) was added to all experimental sample wells. The absorbance at 546 nm was evaluated in a plate reader after allowing it to stand for 10 minutes at room temperature. A blank solution without the test sample was carried out along with standard curcumin. Both the standard and blank solution wells were prepared using the same protocol as of test samples. Graph Pad Prism 6 was operated to compute the nitrite concentration from a variable and sigmoid dose-response curve, and a nonlinear regression analysis (curve fit) was produced to derive IC_{50} values.

SOD Enzyme Catalysis

In SOD enzyme catalysis, metal ion reduction, and superoxide ion oxidation takes place simultaneously, SOD catalyzes the conversion of potentially toxic superoxide to less toxic hydrogen peroxide and molecular oxygen by redox reaction. Samples tested for superoxide dismutase assay have shown the potency to quench superoxide. The WST-1 [2-(4-Iodophenyl)- 3-(4-nitrophenyl)-5-(2,4-disulfophenyl)-2H -tetrazolium, monosodium salt] is a water-soluble salt that is used in the SOD Determination Kit (19160 SOD, Sigma Aldrich purchase), which leads to the formation of formazan dye that is water-soluble when reduced with O_2^-. At 440 nm, by measuring a reduction in color development, which is inversely correlated to the activity of xanthine oxidase (XO) and the rate of oxygen reduction inhibited by SOD, it is feasible to assess the SOD activity as an inhibitory activity. 200 µL of the working solution (WS) and 20 µL of enzyme working solution (EWS) were added to both blank and sample wells in a 96-well microplate previously loaded with 20 µL of the sample and double-distilled water, incubated for

about 20 minutes at 37 °C. With the aid of an optical microplate reader, the absorbance at 450 nm was recorded. The SOD potency was calculated using the formula below. With the aid of Graph Pad Prism 6, using a variable and sigmoid dose-response curve, a nonlinear regression analysis (curve fit) was produced to derive IC_{50} values.[14] The inhibition rate and SOD activity were computed using the equation below:

$$SOD\ activity\ (inhibition\ rate\ \%) = \frac{Absorbance\ (control) - Absorbance\ (test\ sample)}{Absorbance\ (control).} * 100$$

$$SOD\ \frac{mU}{mL} = \frac{SOD\ (nM)}{Absorbance * Reaction\ volume(ml)} * 2$$

Cytotoxic Activities

Counting live cells after staining with the essential dye MTT (3- [4, 5- dimethylthiazol-2-yl]-2, 5-diphenyl tetrazolium bromide) has been used to identify the negative in vitro effects of metal complexes. In medium or salt solutions devoid of phenol red, the water-soluble tetrazolium salt used in the MTT method uses mitochondrial dehydrogenases to gauge the activity of viable cells by yielding a yellowish solution.[15] The dissolved MTT's tetrazolium ring was broken down by the enzyme mitochondrial dehydrogenase of viable cells to create an insoluble purple formazan. To solubilize water-insoluble formazan formed, DMSO was utilized. A spectrophotometric analysis of the resultant purple solution is performed. The amount of formazan produced changes in tandem with a change in cell number, showing the degree of viable cells following MTT dye staining has been employed to assess the harmful effects of metal complexes in vitro.[16,17] A spectrophotometric analysis of the resultant purple solution is performed. The amount of formazan produced changes in direct proportion to the number of cells present indicating the degree of cytotoxic effects inhibited by the metal complexes. Stock cells (cancer cells) from the ATCC were cultured in DMEM/RPMI until confluent. Using a cell-dissociating solute ion [(0.2 percent trypsin ($C_{35}H_{47}N_7O_{10}$), 0.02 percent ($C_{10}H_{16}N_2O_8$) ethylene diamine tetraacetic acid, 0.05 percent glucose ($C_6H_{12}O_6$) in phosphate-buffered saline (PBS)] the cells were broken up after examining cell's vitality they were centrifuged. Additionally, a 96-well plate with 50,000 cells was seeded into each well and cultured for 24 hours in a 5 percent CO_2 environment at 37 °C. The published method was modified for the MTT assay for the metal complexes.[18,19] DMSO was used to dissolve the formazan that had formed after the supernatant was drained from the plates. An absorbance measurement was made using a microplate reader and a 590 nm wavelength.[20,21] The test drug concentrations required to arrest the growth of cells by 50% (IC_{50}) were calculated using the percent inhibition formula and were based on a variable and sigmoid dose-response curve, a nonlinear regression analysis produced with the aid of Graph Pad Prism 6.

Cell Cycle Studies

The production and recombination of nuclear DNA preceding cellular division and mitosis are the two most visible aspects of the cell cycle. The "S" phase and "mitosis" or "M" are used to typically refer to these two cell cycle phases. A temporal time lag or gap between mitosis and the start of DNA synthesis, in addition to the time gap between the end of DNA synthesis and the early part of the S phase and M phase of the cell cycle was noticed when the S phase and M phase of the cell cycle were first explained. Analysis of cell DNA constituents was one of the first uses of flow cytometry. Flow cytometry enables quick evaluation of single cells with statistically significant numbers of cells. The primary concept underlying this technique is the capacity to stoichiometrically stain cellular DNA via scattering of light and fluorescence emission. Propidium iodide was utilized as the DNA-binding dye (PI- DNA-binding intercalating dye).[22] A "narrow" distribution of fluorescence intensities is obtained by flow cytometry analyses in which diploid cells were labeled with PI that stoichiometrically bonds with DNA. In a 6-well plate, 1 x 10^6 cells were sown with 2 ml of medium, and the cells were allowed to grow for 24 hours (RPMI) then they were incubated with complexes prepared in the medium at 25 and 50 mM concentrations after an additional 24 hours of incubation and then the supernatant was carefully discarded to collect the cells from cell pellet following centrifugation for 5 minutes at room temperature at 2000 rpm, again cell pellet was washed once more using the same procedures after being resuspended in 2mL

of 1XPBS (PBS should be 1X to maintain consistent osmolarity of cells). Analogously, the cell pellet was washed once again. The pellet was kept, while the supernatant was tossed away. The cells in the pellet were resuspended in 300 µl of Sheath fluid to fix the cells, a 30X concentrated phosphate buffered saline-based solution that helps break up cell clumping for counting and serves as a disinfectant for microbial contamination of the cell pellet. After that, two batches of 1 mL of ice-cooled 70% EtOH were added drop by drop to stop cell proliferation by dormant cells by gently shaking the mixture. The cells were then incubated overnight at 4 °C. Following cell fixation, centrifugation was carried out for 5 minutes at 2000 rpm to remove ethanol from the cells. 2 ml of cold 1XPBS was used to wash the cell pellet twice. The quantity of the farmed cells was counted after they were frozen. In dark conditions for about 20 minutes, 0.05 g/mL PI and 0.05 g/mL RNaseA in 500 µl of sheath fluid was used to subculture and nourish the cell pellet.[23,24] Using cell BD FACSC caliber software, the ratio of populations of cells in each stage of the cell cycle treated and untreated with various medications was calculated.

Apoptosis of Cancer Cell Lines by Metal Complexes

Early apoptosis is characterized by modifications that ultimately result in the loss of the mitochondrial membrane integrity and emit fluorescence at a wavelength of 590 nm. The emission of the binding dye shifts to 530 nm once the membrane potential is reduced. This change is used to assess the potential of the mitochondrial membrane and the onset of early-stage apoptosis in the cell. DNA fragmentation is a characteristic of the final stage of apoptosis. A severe and uncontrollable form of cell death known as necrosis, it is morphologically characterized by nuclear and oncosis (organellar swelling), as well as plasma membrane rupture. Necrosis can be uncomfortable and lead to an uncontrolled infection. The dying cell spills out its intracellular contents, which include molecules that produce a significant amount of heat leading to an exceedingly fast breakdown of membrane integrity. Whereas necrosis is an abrupt loss of membrane integrity that allows the intracellular contents to flow out, apoptosis is a premeditated suicide cell where the cell destroys itself while preserving the body's normal functioning. Whereas necrosis is an abrupt loss of membrane integrity that allows the intracellular contents to pour out by the dying cell, necrosis is a premeditated suicide cell where the cell kills itself ensuring a smooth functioning of the body. This contains substances that create a large inflammatory reaction in the immune system of the organism and consequently cause tissue damage. Annexin V/PI double-positive cells are late apoptotic signals while PI-positive and Annexin V-negative cells are necrosis signals and Annexin V-positive and PI-negative cells are early apoptotic indications.[25] The process of apoptosis starts when a cell is activated and can develop in several different ways depending on the kind of cell. Cell death and the development of apoptotic bodies mark its conclusion. During an important stage of apoptosis, dying cells develop surface changes that eventually enable phagocytes to recognize and consume these dying cells. Apoptotic cells' surfaces undergo a range of changes, including the ablation of sialic acid residues, the activation of thrombospondin binding sites, and the disclosure of a phospholipid such as phosphatidylserine (PS).[26,27] Phospholipids are asymmetrically distributed between the inner and outer leaflets of the plasma membrane, with phosphatidylserine prevailing on the inner surface toward the cytosol and phosphatidylcholine and sphingomyelin exposed in the outer leaflet of the lipid bilayer PS interface onto an outside surface. There have been instances of PS being exposed to the cell membrane's surface by senescent erythrocytes and activated platelets. In the early stages of apoptosis PS exposure potentially serves as a frequent and early indicator of dying cells. Apoptotic cells expose PS, which is then transmitted to the membrane's outer layer, by compromising the phospholipid asymmetry of their cellular components. The cell membrane is still intact and the cell is in the early stages of apoptosis. Annexin V, a recently discovered cellular protein family that exhibits minimal binding to phosphatidylcholine and sphingomyeline and selectively binds to negatively charged phospholipids like PS in the presence of Ca^{2+} and is an important tool for identifying apoptotic cells.[28,29] Changes in PS asymmetry, as measured by Annexin V binding to the cell membrane, have been discovered before morphological alterations associated with apoptosis and before membrane integrity has been compromised. By conjugating Fluorescein isothiocyanate (FITC) to Annexin V, it is feasible to detect and quantify apoptotic cells on a single-cell basis via flow cytometry. By labeling cells with FITC-Annexin V (green fluorescence) and propidium iodide simultaneously, it is feasible to discriminate between intact

cells, early apoptotic cells, and late apoptotic or necrotic cells (red fluorescence).[30,31] It is possible to quantify the proportion of a population's cells that are actively undergoing apoptosis detecting phosphatidylserine molecules that have moved to the cell membrane's periphery, FITC and an enzyme (Annexin V) quantifies the proportion of cells in a population that are actively going through apoptosis. An annexin V-FITC-stained plasma membrane will be visible in cells that have bound the dye. Red staining indicates damaged cells with compromised membrane integrity (PI). In flow cytometry, light is sent through a channel that experiences both sideward and forward scattering. Annexin V binds to phosphatidylserine as Propidium iodide binds to broken-down DNA when a cell's membrane permeability is compromised. Excitation emission fluorescence is a sign that a metal complex has succeeded in stopping the development of a cancer cell. Annexin V binds to phosphatidyl serine whereas both fluorescent tags, propidium iodide, and annexin V, attach to damaged DNA when a cell's membrane permeability has been impaired. If a metal complex has stopped the growth of a cancer cell, excitation-emission fluorescence can be seen; this indicates that the cell is apoptotic. In a 6-well plate, 1 X 10^6 cells per well were plated with the corresponding medium 1% PenStrep and 10% FBS (mixture of penicillin G and streptomycin). The cells were then kept at 37 degrees Celsius with 5 percent CO_2 overnight. The original media were swapped out by media containing varying amounts of metal complex solutions. The cells were cultivated for 24 hours after being treated. Under typical circumstances, Cells were reconstituted in binding buffer (1.4M sodium chloride, 25 mM Calcium chloride solution, 0.2 µM sterile filtered 0.1M Hepes [(4-(2-hydroxyethyl)-1-piperazineethanesulfonic acid) at p^H 7.4],) following two cold PBS washes and a 5-minute centrifugation at 2000 rpm. After removing the supernatant 500 µL of cell solution was added to a fresh FACS tube (Fluorescence Activated Cell Sorting/ flow cytometry tube), which contained 1 x 10^6 cells/ml. The tubes were filled with 10 µL of PI and 5 µL of Annexin V following 20 minutes of incubation in the dark at room temperature after the cells were resuspended. A flow cytometry examination was then performed on the cells.[32,33]

Antimicrobial Activities

The potency of the synthesized mononuclear, homo binuclear, and hetero binuclear metal complexes along with its parent ligand **1** was tested for a few types of fungi and bacteria by using a conventional disc diffusion method on nutrient agar slants by modifying the reported method.[34,35] M. luteus, E. coli, E. feacalis, P. aeruginosa, and S. aureus were inoculated using peptone broth, and the injections were inoculated for 30 hours at 37 °C. While potato dextrose agar was prepared and inoculated with C. albicans, A. niger, and F. oxysporium cell suspensions, cultures were then rested for 48 hours at 27°C and were adjusted to 1-2x 10^5cells/ml. Soyabean Casein Digested agar plates and Potato Dextrose agar plates (90 mm) were inoculated and added with ciprofloxacin and itraconazole (25µl) respectively and a control (25µl) was added to the agar plates. Standard antibiotic ciproflaxin and one test sample (50 g mL^{-1} and 100 g mL^{-1}) were added to each test plate for bacterial strains while standard itraconazole and one test sample were added to each test plate for fungal strains. All discs were inoculated with DMSO as the negative control. According to the molecular weight, a 10Mm solution containing metal complexes 2, 3, and 4, as well as their parent ligand 1, was prepared and deposited to the test plate and inoculated 24 hours and 48 hours for bacterial strains and fungal strains at 37 ^{0}C and 27 ^{0}C, respectively. After incubation, the petri dish was checked for an inhibition zone. The minimum inhibitory concentration (MIC) for metal complexes that have shown inhibitory activity is calculated by operating Graph Pad Prism 6 to analyze a nonlinear regression by the variable and sigmoid dose-response curve. Obtained data are fitted using a series of approximations. A dose-response curve was prepared to deploy positive controls in agar well diffusion studies for the individual strains using ciproflaxin and itraconazole for bacterial and fungal strains respectively.

RESULTS AND DISCUSSION

FT-IR Spectroscopy

The IR spectra of free ligands (Fig.-1) and complexes (Fig.-2 to 4) in the 4000-100 cm^{-1} region include essential information regarding the coordination of metal to the ligand. Table-1 contains a collection of significant peaks. The IR spectrum of the free ligand dmedox shows carboxyl and amide stretching vibrational bands as steep peaks in the ranges of 1666 cm^{-1} and 3302 cm^{-1} respectively.[25] In contrast to the

free ligand, complex (2) exhibits a hypsochromic shift of carbonyl (C=O) and (N-H) at 1582 cm^{-1} and 3356 cm^{-1}, respectively.[36] The mononuclear complex is generated by coordination with deprotonated amide nitrogen to the metal ion, which may account for why the (C=O) of binuclear complexes (3) and (4) fall around (C=O) of free ligand. In the protonated species of mononuclear complex, the amide I band dislocates markedly towards either a lower or higher wave number. In contrast to the corresponding binuclear complexes this is due to the following reasons, deprotonated amide nitrogen and metal ion coordinates to form a mononuclear metal complex. The amide I band displaces significantly toward the greater or lesser wave number and the amide I band degenerates and moves back to its initial position when the bridging ligand for two metal ions is oxamide dianion. In comparison to the corresponding mononuclear metal complexes, the C=O binuclear complexes have a higher bond order. Generally, in binuclear complexes, this dislocation in shift confirms the oxamido bridge. This displacement is frequently cited as clear evidence for the presence of an oxamido bridge in nuclear complexes.[37] In complex 2, 3, and complex 4, bending vibrations remarked in the ranges 483 cm^{-1}, 420 $cm^{-1,}$ 470 cm^{-1}, 401 cm^{-1}, and 429 cm^{-1} are respectively associated with ν(M-N) bonding in the corresponding complexes (2), (3), and (4). These details show how metal ions are coordinated to the deprotonated oxamido group in dmedox. In addition to that, signals at 545 cm^{-1}, 513 cm^{-1}, and 558 cm^{-1} are ascribed for ν(M-O)[10] bonding in complexes (2), (3) and (4) respectively, the coordinated ionic peak found in metal complex **4** is due to vibration of C_{2v} symmetry of the nitrate group, wave number difference of two highest peak (ν_a~ν_b) of nitrate is around ~180 in complex 4 which gives evidence that coordinated nitrate is bidentate. Signals at 1555 cm^{-1} and 1512 cm^{-1} are associated with the coordination of 1,10-phenanthroline as a terminal ligand whereas peaks at 1382 cm^{-1} are related with ionic nitrate ν(NO_3^-),[38] in metal complexes 3 and 4 respectively.[39] In complex 2, the bands at 1130 cm^{-1}, and 623 cm^{-1} are ascribed to perchlorate ion ν(ClO_4^-).[40] These spectral data are in agreement with NMR spectra and molar conductivity data.

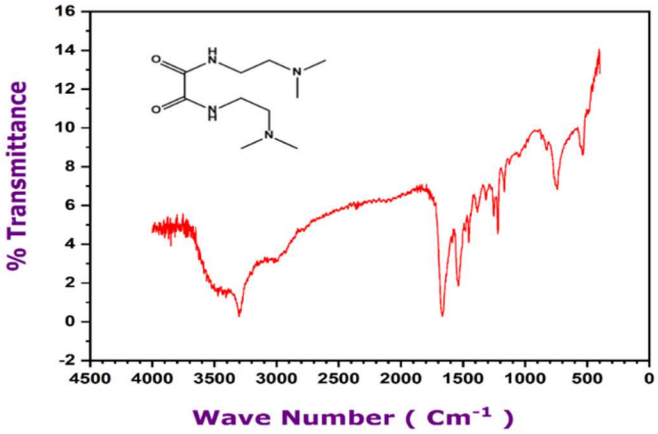

Fig.-1: IR Spectrum of dmedox 1 in KBr Disc

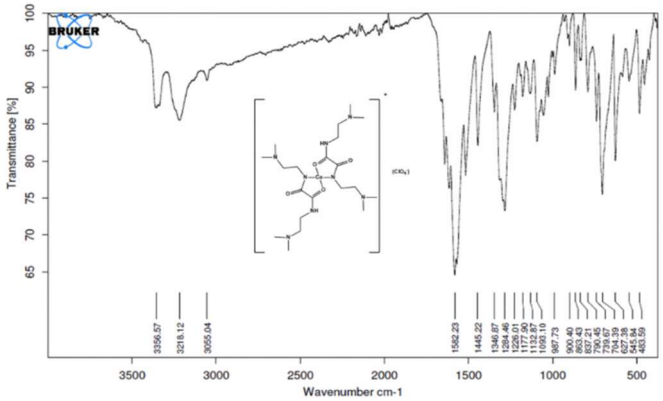

Fig.-2: IR Spectrum of Complex 2 in FT-IR

^{1}H-NMR Spectroscopy

Proton NMR spectra of the complexes provided some specific revelations in exploring the coordination nature of metal complexes. ^{1}H-NMR spectra of 1, 2, 3 and 4 exhibit δ values in the region 1.02-3.49 ppm for alkyl –CH_2 protons, chemical shift values falling in the range 8.32 to 8.48 ppm corresponds to amide –NH protons, chemical shift values in the range 7.3 to 8.9 ppm corresponds to aromatic protons of heterocyclic base of 1,10-phenanthroline (Fig.-5).[41] Complex 2 exhibits δ values in the range of 1.25 to 3.12 ppm and 8.32 to 8.48 ppm attributed to alkyl –CH_2 protons and –NH protons respectively.

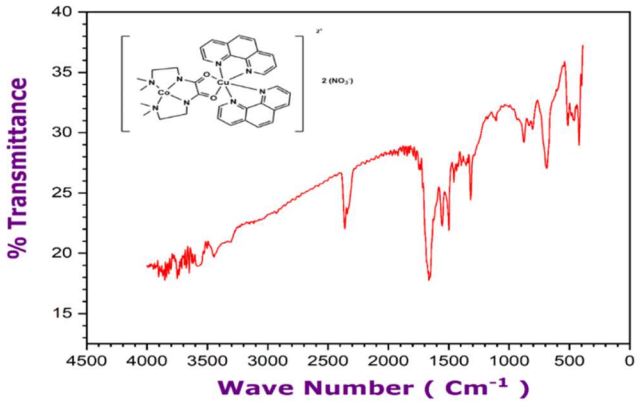

Fig.-3: IR Spectrum of Complex 3 in KBr Disc

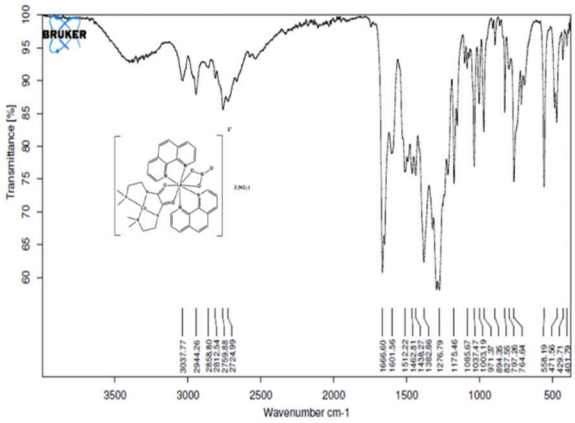

Fig.-4: IR Spectrum of Complex 4 in FT-IR

Table-1: IR Spectral Data for 1, and it's Mononuclear 2, Hetero Binuclear 3 and 4 Metal Complexes

Code	υ(C=O)	υ(N-H)	υ(C=N)	υ(M-O)	υ(M-N)	υ(ClO_4^-)	υ (NO_3^-) (ionic)	υ (NO_3^-) (coordinated)		
								υ_a	υ_b	υ_c
1	1666	3302	-	-	-	-	-	-	-	-
2	1582	3356	-	545	483	1132,627	-	-	-	-
3	1664	-	1555	513	420,470	-	-	-	-	-
4	1666	-	1512	558	401,429	-	1382	1462	1276	1085

The appearance of –NH protons provides evidence for the complexation of mononuclear complex 2 with amide –NH protons (Fig.-6).[42] Complex 3 exhibits δ values in the range 1.4 to 2.0 ppm and 7.3 to 8.6 ppm attributed to alkyl –CH_2 protons and aromatic protons of 1,10-phenanthroline respectively. The absence of amide –NH protons concerning mononuclear complex 2, suggests the deprotonation of the amide group and coordination with metal ions.[43] Chemical shift value in the range 7.3 to 8.6 ppm attributes the presence of aromatic protons of 1,10-phenanthroline in the coordination sphere, these results indicate the formation of binuclear complex 3 (Fig.-7). Complex 4 has chemical shift values of alkyl –CH_2 and aromatic protons of 1,10-phenanthroline at 1.5-1.6 ppm and 7.6-8.9 ppm respectively (Fig.-8). ^{1}H-NMR spectra revealed the absence of amide –NH protons concerning mononuclear complex 2, evidence for the

coordination of amide –NH protons with a metal ion, and the presence of aromatic protons of 1,10-phenanthroline, confirms the formation of binuclear complex 4 by deprotonation of amide –NH protons. The peaks of the 1,10-phenanthroline base appear to be multiplet due to Protons that are magnetically non-equivalent present in two different ligands.[44]

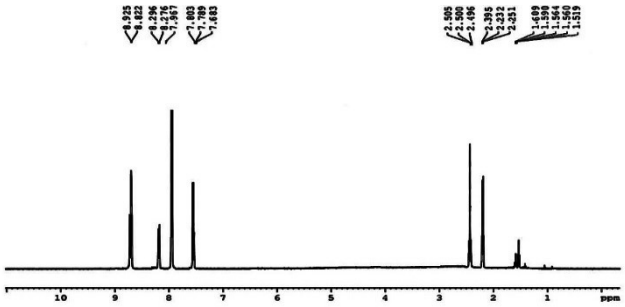

Fig.-5: ^{1}H-NMR Spectrum of Ligand 1 in DMSO-*d6* using TMS as Standard

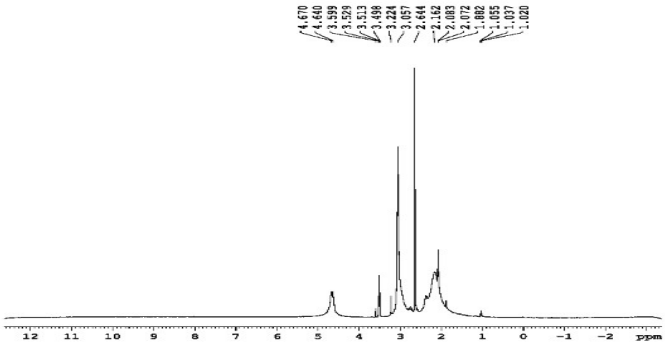

Fig.-6: ^{1}H-NMR Spectrum of Complex 2 in DMSO-*d6* using TMS as Standard

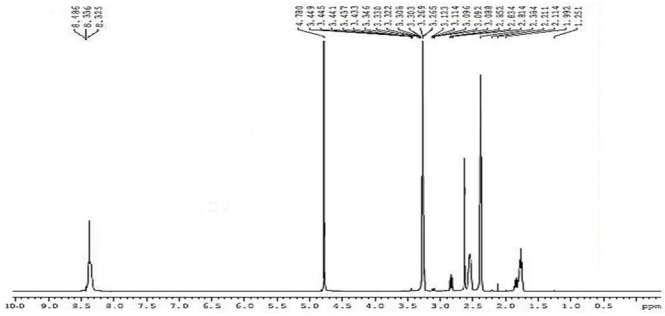

Fig.-7: ^{1}H-NMR spectrum of complex 3 in DMSO-*d6* using TMS as standard.

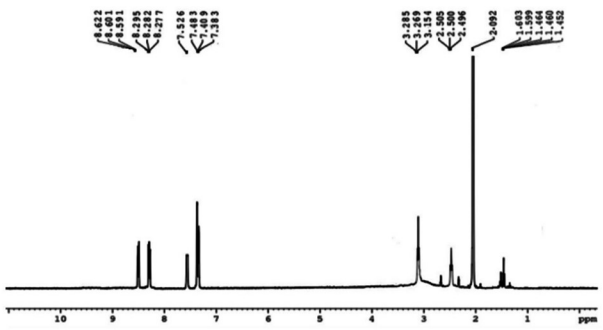

Fig.-8: ^{1}H-NMR Spectrum of 4 in DMSO-*d6* using TMS as Standard

UV-Visible Absorption Spectroscopy

Table-2 contains the information on the electronic absorption spectral information of mono- and hetero-binuclear complexes synthesized from ligand 1 (Fig.-9-11). The intra-ligand charge transfer may be the cause of the strong band at 244 nm. Intense peaks seen between 428.9 nm and 229 nm are ascribed to ligand-to-metal (LMCT) or metal-to-ligand charge (MLCT) transitions, respectively. Low-intensity broad bands obtained in the region of 644.5 nm to 524 nm may be associated with d-d transitions and LMCT or MLCT transfer may be responsible for the strong absorption bands found at 430 nm and 283 nm.[10] In complex 4, the absorption bands at 340 and 211 nm may be related to metal-to-ligand or ligand-to-metal charge transfer, respectively. Intraligand transitions may obscure other expected transitions.[45] In bimetallic complexes a decrease in the planarity of the metal oxamide chromophore [MN_4] results in a higher wavelength of the absorption band and an increase in the frequency of d-d transition increases the value of the molar absorption coefficient. We noticed a broad d-d band that was unresolvable even though the two metal ions are present in two distinct coordination sites. As each of the metal complexes was successfully isolated in powder form, IR, ESI-MS, NMR, and molar conductance experiments have further substantiated the plausible structures of the complexes.[46,47] A Time-dependent stability study of all three mononuclear hetero and binuclear metal complexes (Fig.-12-14) was conducted in solvent medium DMSO/DMF and H_2O ($V_{DMSO/DMF}$: V_{H2O} = 1:9) over 6h revealed that all the complexes are stable in this medium which further facilitated to carry out biological assay in this standard medium.

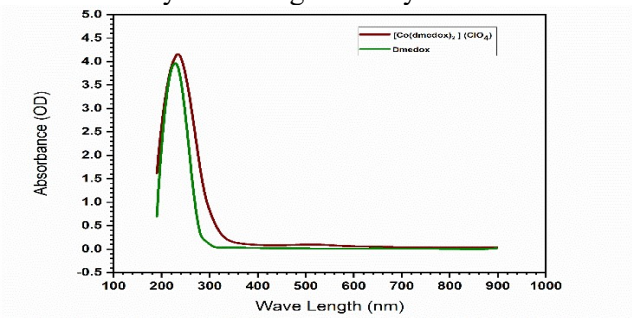

Fig.-9: UV-Visible Absorption Spectra of 10^{-3} M Solutions of Ligand 1 and Complex 2 in DMSO and H_2O (V_{DMSO}: V_{water} = 1:9)

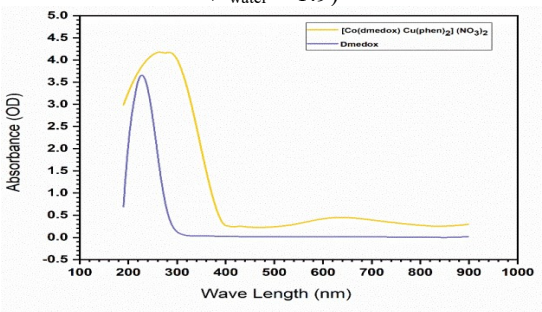

Fig.-10: UV-Visible Absorption Spectra of 10^{-3} M Solutions of Ligand 1 and Complex 3 in DMSO and H_2O (V_{DMSO}: V_{water} = 1:9)

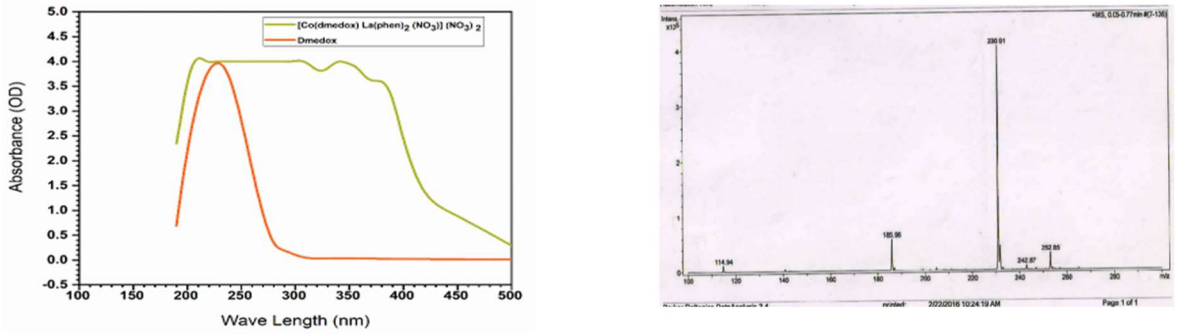

Fig.-11: UV-Visible Absorption Spectra of 10^{-3}M Solutions of 1 and 4 in DMF and H_2O (V_{DMSO}: V_{water} = 1:9)

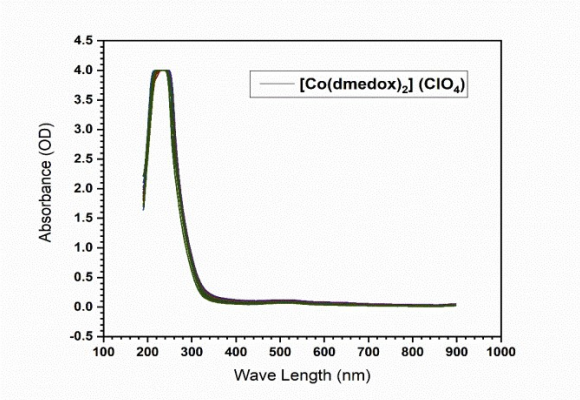

Fig.-12: Time-Dependent Stability Study of Complex 2 by UV-Visible Absorption Spectroscopy Over 6h in DMSO and H_2O (V_{DMSO}: V_{water} = 1:9)

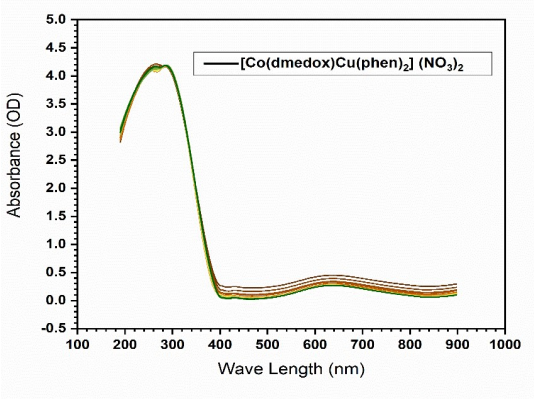

Fig.-13: Time-Dependent Stability Study of Complex 3 by UV-Visible Absorption Spectroscopy Over 6h in DMSO and H_2O (V_{DMSO}: V_{water} = 1:9)

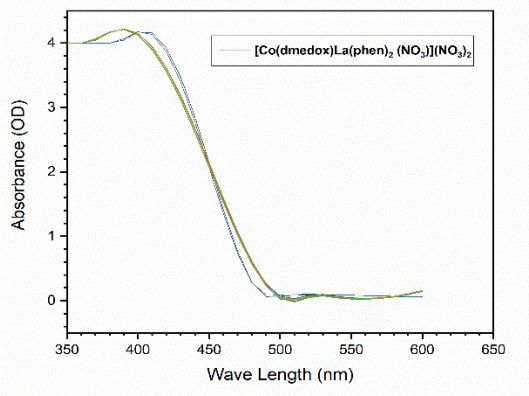

Fig.-14: Time-Dependent Stability Study of Complex 4 by UV-Visible Absorption Spectroscopy Over 6h in DMF and H_2O (V_{DMSO}: V_{water} = 1:9)

Table-2: Electronic Spectral Data of Ligand 1 and its Corresponding Complexes 2, 3, and 4

	UV (nm)	λ_{max}/nm (ε/$dm^{-3}m^{-1}cm^{-1}$)
Code	d-d	CT
1		244 (1059)
2	520.0 (842)	229 (371), 428.5 (694)
3	632.5 (757)	283 (338), 430.0 (514)
4		211 (216), 340.0 (349)

ESI-MS Spectroscopy

Fig.-15 has shown base peak value at 230.9 a.m.u corresponding to M^+ peak this confirms the formation of ligand 1. Fig.-16 has shown a base peak value at 616.2 a.m.u corresponding to the M^+ peak this

confirms the formation of complex 2. Figure-17, the base peak value in mass spectra has an m/z value of 356.6 a.m.u. that which corresponds to $[M+H-2(NO_3^-)]^+$ ion peak where $M=[Co(dmedox)Cu(phen)_2]^{2+}$ ion which indicates the formation of complex 3. Fig.-18 has m/z value 425.3 a.m.u. which corresponds to $[M+H-2(NO_3^-)]^+$ ion peak where $M=[Co(dmedox)La(phen)_2(NO_3)]^{2+}$ ion which signifies the structural formation of complex 4. The ESI-MS spectra recorded in methanol for ligands and their respective complexes confirm the formation of ligand and their respective ionic complexes since depending on the experimental conditions positively charged ions like H^+, Na^+, K^+ or solvent molecule interferes in ESI-MS mode which may show up as background ions with the m/z peak.[48,49] m/z values of mass spectra of 1, 2, 3, and 4 are in correspondence with FTIR, NMR, spectral data along with molar conductance values, and CHNS analysis, the formation of complexes can be concluded. The spectral data are within the predicted range and are correlated with the corresponding synthesized ligand and its complexes. According to tests of molar conductance, the newly synthesized complex 2 is a 1:1 electrolyte in DMF solvent, whereas complexes 3 and 4 are 1:2 electrolytes.

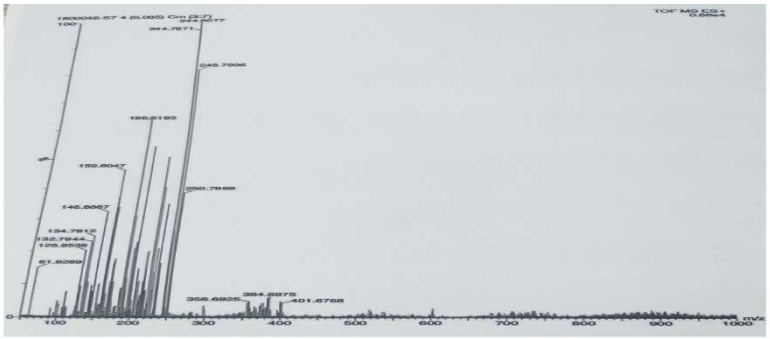

Fig.-15: ESI-Mass Spectrum of Ligand 1 in Positive Ion Mode in CH_3OH

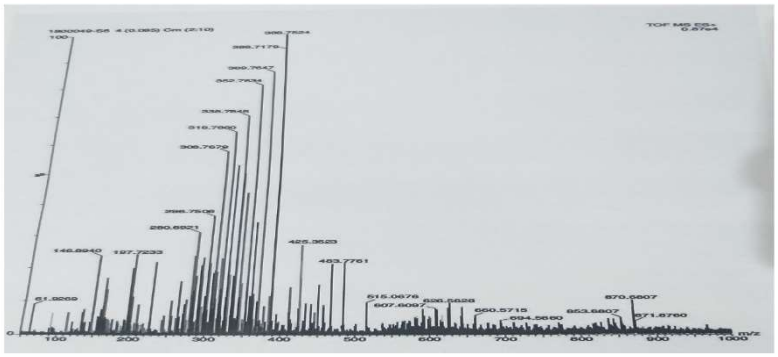

Fig.-16: ESI-Mass Spectrum of Complex 2 in Positive Ion Mode in CH_3OH

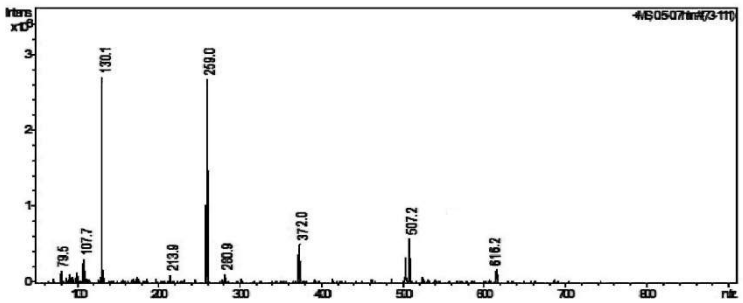

Fig.-17: ESI-Mass Spectrum of Complex 3 in Positive Ion Mode in CH_3OH

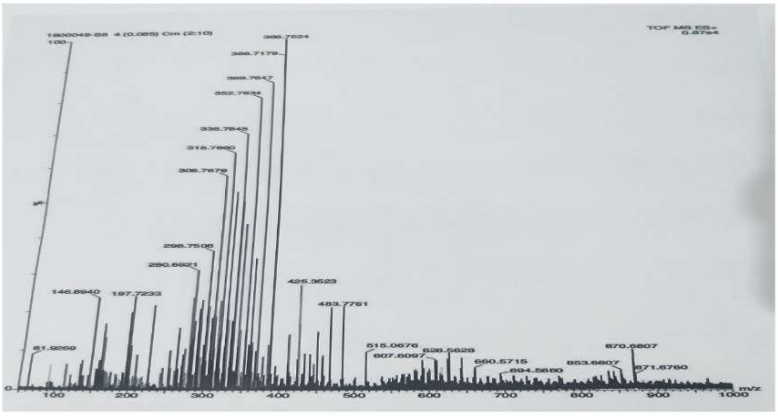

Fig.-18: ESI-Mass Spectrum of Complex 4 in Positive Ion Mode in CH_3OH

Calf thymus- Deoxyribonucleic Acid Binding Studies UV-Visible Absorption Titration

Absorption titration curves were constructed by UV-visible absorption titration technique for metal complexes 2, 3, and 4 using origin version 6**.** Titration curves were constructed for the complex without DNA (ε_f) and the complex when fully bound to DNA (ε_b). A_{obs}/[complex] was used to calculate ε_a The following equation was used to fit the data, where, the y-intercept is $1/[K_b(\varepsilon_b - \varepsilon_f)]$ and $1/(\varepsilon_b - \varepsilon_f)$ is slope. K_b was calculated by dividing the slope by intercept. Plots comparing $[DNA]/(\varepsilon_a - \varepsilon_f)$ and [DNA], were used to estimate binding constants which were found to be $1.54 \times 10^3\ M^{-1}$ (r = 0.7509) (2), $3.07 \times 10^3\ M^{-1}$ (r = 0.9075) (3) and $3.61 \times 10^3\ M^{-1}$ (r = 0.8630) (4). (Table-3) in the order: 2> 4 > 3. Fig.-19-21 demonstrates how the quantity of CT-DNA in the metal complexes alters absorption intensities spectral bands about the linear fit curve response.

Complex 2 has a specific spectrum alteration that exhibits hyperchromism which indicates complex 2 is bound to DNA either by electrostatic interaction mode or by groove binding interaction mode.[50] Complexes 3 and 4 include expanded planar phenanthroline bases, which promote non-covalent interactions between DNA and the metal complexes.[51-53] Complex 2 has a specific spectrum alteration that exhibits hyperchromism and a very slight bathochromic shift (~4 nm). This may be brought on by a repercussion between the DNA base pairs' π-orbitals and the π*-orbitals of intercalated complexes, which lowers the π - π * bathochromic shift induced by transition energy. Additionally, electrons in the π - π* orbital are partially filled as a result of coupling, which lowers transition probabilities and induces hypochromism.

Table-3: Intrinsic Binding Constant of Metal Complexes 2, 3, and 4

Complex	K_b (M^{-1})
2	1.54×10^3
3	3.07×10^3
4	3.61×10^3

K_b = Intrinsic binding constant (M^{-1})

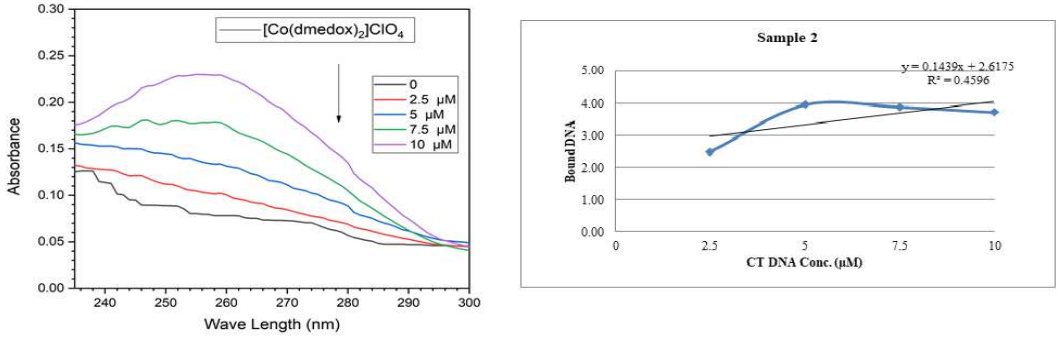

Fig.-19: Titration Curves of Complex 2 by UV-Visible Absorption Spectroscopy; Buffered (pH = 7.2) at 25 ˚C Representing Free and Fully Bound Complex

CT-DNA Binding by Gel Electrophoresis

DNA binding experiments suggest complexes are binding to DNA through intercalation. Evaluation of binding of CT-DNA with metal complexes by gel electrophoresis shows that the heterogeneous binuclear complex 4, with mixed ligands oxamide and 1,10-phenanthroline, has 87.23 % highest percentage of binding efficiency vs its parent ligand (lane 5). Because of the structure-activity relation, these newly synthesized metal complexes could be useful diagnostic and therapeutic agents in the pharmaceutical industry,[54-55] the outcomes are depicted in Fig.-22 and listed in Table-4.

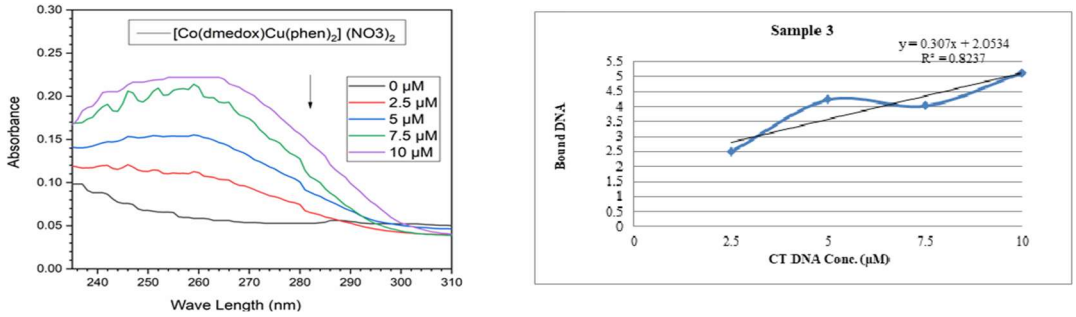

Fig.-20: Titration Curves of Complex 3 by UV-Visible Absorption Spectroscopy; Buffered (pH = 7.2) at 25 ˚C Representing Free and Fully Bound Complex

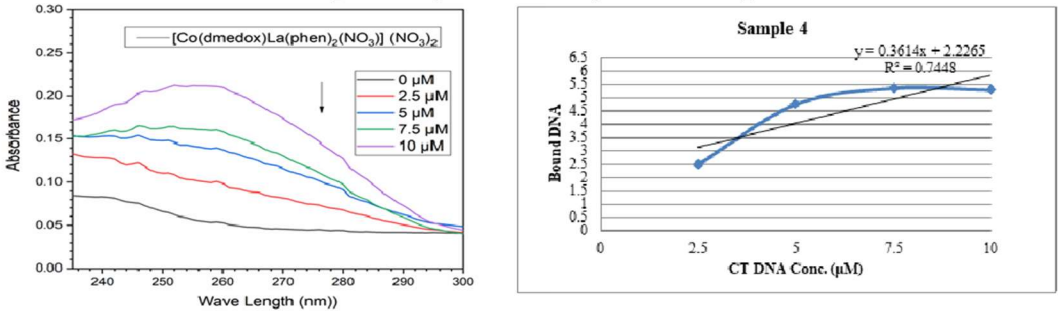

Fig.-21: Titration Curves of Complex 4 by UV-Visible Absorption Spectroscopy; Buffered (pH = 7.2) at 25 ˚C Representing Free and Fully Bound Complex

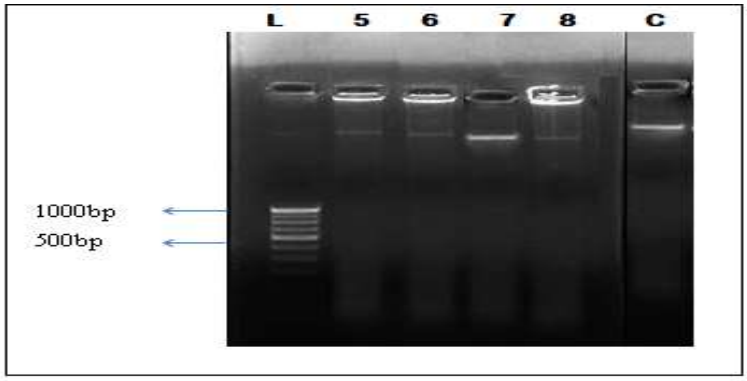

Fig.-22: Agarose Gel Electrophoresis Picture Displaying Binding Efficiency of CT-DNA by 10 µM Ligand 1 and Complexes 2, 3, and 4 Buffered by 5 mM Tris-HCl and 50 mM Sodium Chloride, pH = 7.2) at 25 ˚C

Table-4: Band Intensity and % of Binding Efficiency of Ligand 1 and its Metal Complexes 2, 3, and 4

Complex	Band intensity (RFU)	Binding Efficiency (%)
1	9621.30	23.45
2	3365.48	73.22
3	2849.99	77.32
4	1604.28	87.23

[NaCl] = 5 mM; [Tris-HCl] = 50 mM; [Complex] = 10 µM

Antioxidant Activities

DPPH Free Radical Quenching Activity

Metal complexes and their associated ligands were tested for DPPH dosing to discover novel antioxidants (Fig.-23). When compared to the natural anti-oxidant quercetin, the samples showed good radical scavenging efficacy. Antioxidants quench the stable purple color oxidant DPPH, [1,1-diphenyl-2-picryl hydrazyl], into the colorless compound 1,1-diphenyl-2-picryl hydrazine, this has an absorption of 590 nm, stable free radical with purple color is reduced by antioxidants to colorless DPPH to 1,1-diphenyl-2-picryl hydrazine, which is measured at an absorbance of 590 nm. The sweeping activity of free radicals by these complexes can be associated with the presence of electron-releasing $–CH_2$ groups or due to the presence of hydrogen donating –NH groups however the also, the capability of metal complexes to destroy free radicals may be mediated through charge transfer between metal ligands. The molecular pathway for this, however, is unclear 1 and 2 have shown inhibition lesser than 50% whereas heterogeneous bimetal complexes 3 and 4 have shown notable activity with an IC_{50} value of 17.33 μgmL^{-1} and 37.49 μgmL^{-1}.

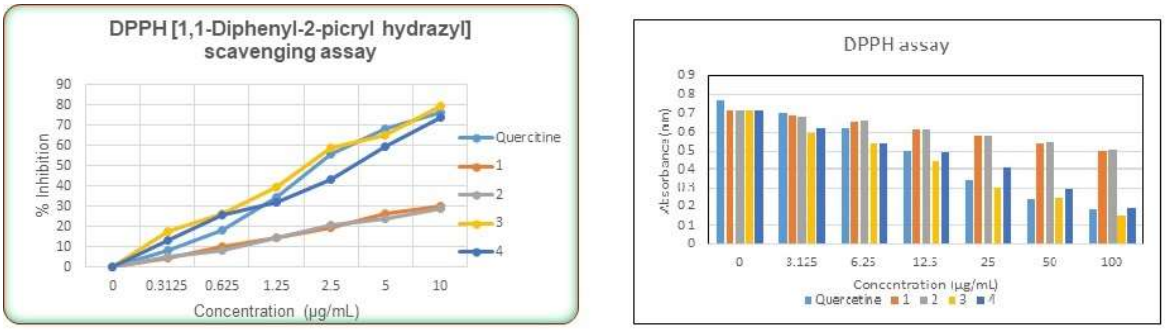

Fig.-23: Concentration Versus % Inhibition Plot for DPPH Radical Scavenging Activity Compared with Positive Control Quercetin of Ligand 1 and its Metal Complexes 2, 3 and 4 and Bar Diagram Representing Concentration Versus Absorbance Plot of Ligand 1 and its Metal Complexes 2, 3 and 4

Nitric Oxide Scavenging Activity

Mono nuclear metal complex 2, binuclear complex 3 and 4 along with ligand 1 treated at 320 μgmL^{-1} exhibited 20.5µM, 33.5 μgmL^{-1}, 555.5 µM and 708.0 μgmL^{-1} nitric oxide content respectively among the tested complexes 3 and 4 exhibited moderate nitric oxide scavenging activity (Fig.-24). When sodium nitroprusside reacts with water (pH 7.0), it produces a nitric oxide free radical by generation of nitrite ions with oxygen interaction. Oxygen and nitric oxide scavengers compete to stop the generation of nitric oxide, being oxidized to the nitrite ion. Griess reagent, an inactive dye, reacts with the nitrite ion to produce a dark purple complex. The intensity of the generated color was measured using absorbance at 546 nm. The intensity of the produced color was assessed by measuring absorbance at 546 nm.[56]

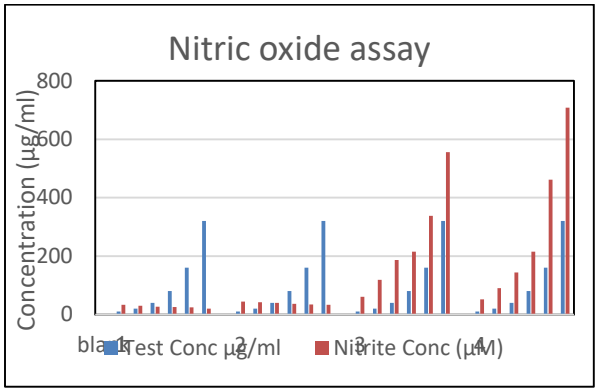

Fig.-24: Bar Diagram Representing Concentration of Sample Versus Scavenged Concentration of Nitrite Ion Plot of Ligand 1 and its Metal Complexes 2, 3 and 4 for Nitric Oxide Radical Scavenging Activity Compared with Positive Control Curcumin

Superoxide Dismutase Assay

Metal ion reduction and superoxide ion oxidation occur simultaneously in SOD enzyme catalysis. SOD catalyzes the redox reaction that converts potentially toxic superoxide to less toxic hydrogen peroxide and molecular oxygen. The ability to quench superoxide was determined in samples tested for superoxide dismutase assay. Mono nuclear metal complex 2, exhibited 4.13 UmL^{-1} binuclear complex 3 exhibited 6.62 UmL^{-1}, and hetero binuclear metal complex 4 exhibited 8.19 UmL^{-1} whereas ligand 1exhibited 1.71UmL^{-1}. In comparison to the parent ligand, all the complexes exhibited moderate quenching activity against superoxide free radicals (Fig.-25).

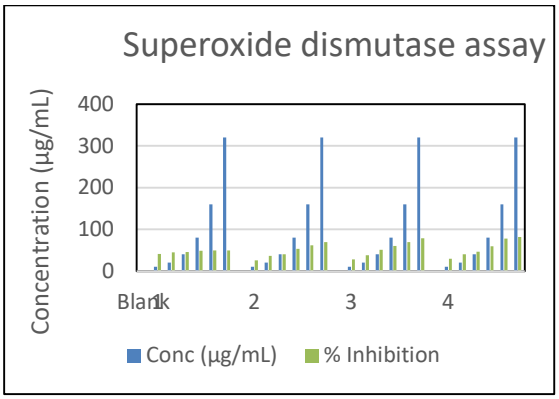

Fig.-25: Bar Diagram Representing a Concentration of Sample Versus % Inhibition Plot of Ligand 1 and its Metal Complexes 2, 3, and 4 for Nitric Oxide Radical Scavenging Activity Compared with Positive Control Standard SOD

Antimicrobial Activities

A bacterium with thick, mesh-like membrane peptidoglycan is termed a gram-positive bacterium, and a bacterium without peptidoglycan is termed a gram-negative bacterium. Antibiotics which can inhibit both types of bacteria a promising agent for medicinal use. By using the well diffusion method all the mononuclear and hetero binuclear metal complexes were screened for antimicrobial activity (10 mM, 25 µL). It was found that complexes 2 and 3 are negative (zone of inhibition was not observed) towards all the microorganisms while heterogeneous bimetal complex 4 has shown good antibiotic activity against gram-positive and gram-negative bacterial strains and has also shown antifungal activity against fungal strain Candida albicans, whereas against fungal strains Aspergillus niger and Fusarium oxysporium antifungal activity was not observed in tested concentration. It is important that the metal complex used as an antimicrobial drug inhibit cell proliferation at lower drug concentrations otherwise it may lead to metal toxicity inside the living system. In this perspective, compared to the parent ligand which is negative towards all bacterial and fungal strains, complex 4 has exhibited good antimicrobial activity. The collegial effect of oxamide –C=O and N donor atoms of heterocyclic base 1,10-phenanthroline with Co(II) and Cu(II) metal ions influence the antimicrobial activity of the metal complex at lower drug concentrations. When oxamide -C=O is coordinated with metal ions and N donor atoms of heterocyclic bases, the polarity of the metal atom is lowered by sharing a positive charge with the donor groups of the ligand (chelation), which may result in -electron delocalization. This increases the lipophilicity of the complexes, allowing them to pass through the lipid membranes of the cell wall. N,N-heterocyclic base 1,10-phenanthroline may amplify the chelating effect on metal ions, lowering their polarity and causing the electrons to delocalize throughout the chelate ring.[57,58] By which bacterial growth is constrained as a result of the altered normal physiology, impaired enzyme metabolism, and decreased permeability of bacterial cell walls. Oxygen and nitrogen atoms required for enzyme activity are deactivated during chelation. Metal complex come in contact with the microorganism cell wall disrupts the cell membrane integrity and blocks the binding sites of enzymes thus inhibiting the metabolism of the cell and obstructing the microorganism proliferation. All the mononuclear, hetero binuclear metal complexes were screened for antimicrobial activity (10 mM, 25 µL). It was found that complexes 2 and 4 are negative (zone of inhibition was not observed) towards all the microorganisms while heterogeneous bimetal complex 3 has shown good antibiotic activity against all the tested bacterial and also against fungal strain, whereas

against fungal strains *Fusarium oxysporium* and *Aspergillus niger* antifungal activity was not observed in tested concentration. It is important that the metal complex used as an antimicrobial drug inhibit cell proliferation at lower drug concentration otherwise it may lead to metal toxicity inside the living system. In this perspective, compared to the parent ligand which is negative towards the entire bacterial and fungal strains complex 3 has exhibited good antimicrobial activity. Complex 3 has minimum inhibitory concentration (MIC) at 62.5, 125, and 62.5 μgmL^{-1} for bacterial strains (gram-positive); *Micrococcus luteus, Staphylococcus aureus,* and *Enterococcus feacalis* respectively. The determined minimum inhibitory concentration for gram-negative bacteria was found to be 62.5 $\mu gmL^{-1}$and 31.25 μgmL^{-1} for *Pseudomonas*, *Escherichia coli*, and *aeruginosa* (gram-negative) respectively. MIC of complex 3 for *C. albicans* fungal strain was found to be 125 μgmL^{-1}. The collegial effect of oxamide –C=O and N donor atoms of heterocyclic base 1,10-phenanthroline with Co(II) and Cu(II) metal ions influence the antimicrobial activity of the metal complex at lower drug concentrations.[59,60] The antimicrobial activity is shown in Fig.-26 and Fig.-27 and the values of the zone of inhibition are tabulated in Table-5.

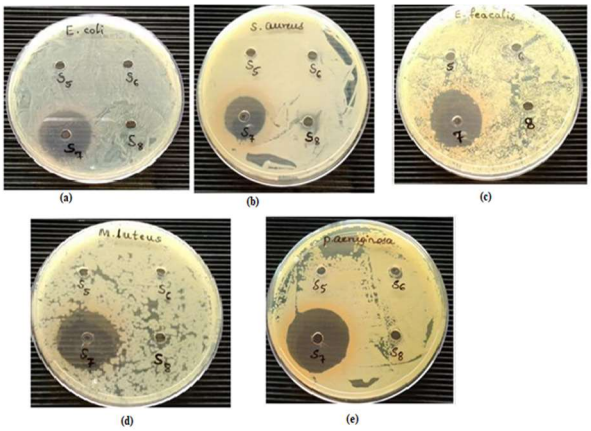

Fig.-26: Metal complex 3 induced zone of suppression Of *E. coli* (a), *S.aureus* (b), *E.feacalis* (c) *and M.luteus* (d)*;* S-standard (Ciprofloxacin); C –Control (DMSO) S5 = Ligand 1; S6 = 2; S7 = 3 and S8 = 4

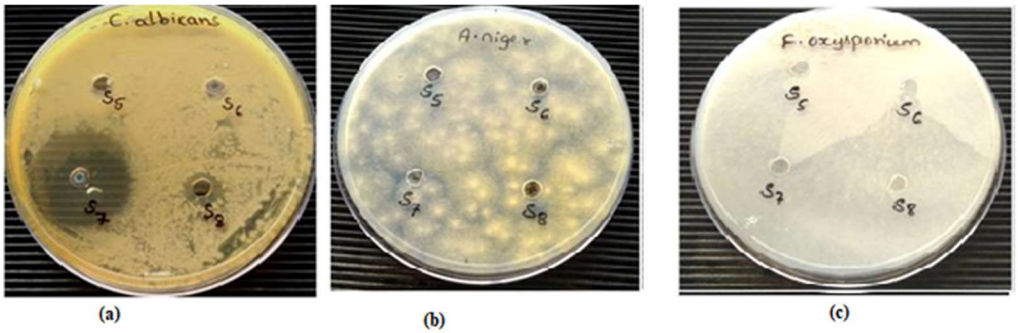

Fig.-27: Metal Complex 3 Induced Zone Of Suppression Of *C.Albicans* (A), *A.Niger*; (B) and *F.Oxysporium* (C)*;* S-Standard (Ciprofloxacin); C –Control (DMSO); S5 = Ligand 1; S6 = 2; S7 = 3 And S8 = 4

Table-5: Zone of Inhibition Induced by Complex 3 And Its MIC Value by Micro Broth Dilution Technique Using Culture Medium: Peptone and Potato Dextrose Broth for Respective Culture with Sample Test Concentrations 100, 50, 25, 12.5, 6.25, 3.125, 1.56% of Against Standard Ciproflaxin; For Bacterial Strain and Itraconazole; For Fungal Strains

Test Organisms	Zone of inhibition(mm)	MIC (μgmL^{-1})
E. coli	28±0.0	62.5
S.aureus	21±0.0	125
E.feacalis	26±0.0	62.5
M.luteus	27±0.0	62.5

P.aeruginosa	31±0.0	31.2
C.albicans	28±0.0	125
A.niger	-	-
F.oxysporium	-	-

Cytotoxic Activities

The samples were tested for cytotoxic activity against HT-29 cell lines, 3 and 4 exhibited IC_{50} values of 32.45 µgmL^{-1} and 35.16 µgmL^{-1} respectively whereas the IC_{50} value for 2 was not calculated due to lesser inhibition. Hetero binuclear complexes exhibit good cytotoxic activity comparatively with parent ligand 1 which exhibited 62.29 µgmL^{-1} IC_{50} value (Fig.-28-30). Transition metals and d-block metals in their complex state exhibit cytotoxic activities due to properties like charge variation, coordination, bonding, metal-ligand interactions, redox activity, and partially filled outer orbitals, etc., This is due to metal cytotoxicity as well as the covalent and noncovalent DNA binding properties of transition metal complexes. In covalent binding, the complex labile ligand is substituted by a nitrogen base of DNA, such as guanine. Intercalated, electrostatically bound, and electrostatically attracted cationic metal complexes are found in the major or minor grooves of the DNA helix.[61]

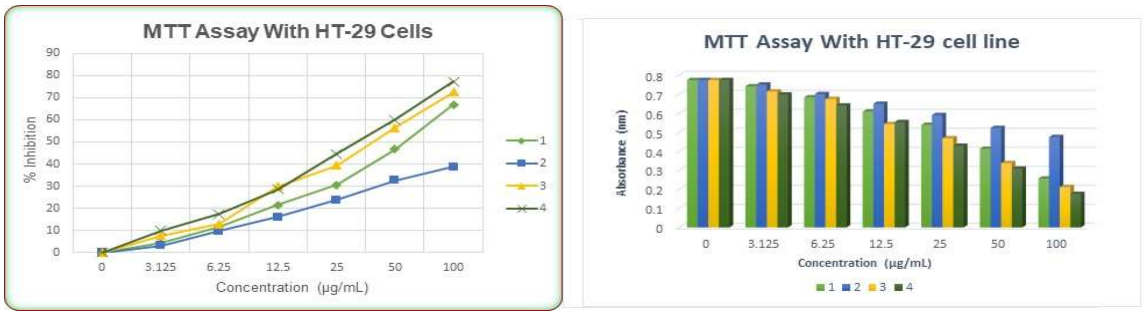

Fig.-28: Graphical Representation of Toxic Activity of Tested Metal Complexes Versus Different Concentration of Metal Complexes 2, 3, and 4 and its Parent Ligand 1 and Plot Exhibiting the Effect of Absorbance Measured Along with Various Doses of the Ligand and Metal Complexes Using the MTT Assay Method concerning HT-29 Cell Lines

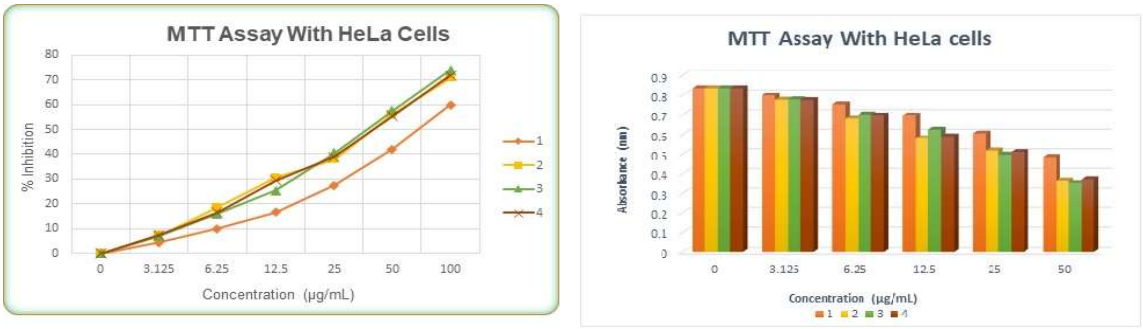

Fig.-29: Graphical Representation of Toxic Activity of Tested Metal Complexes Versus Different Concentration of Metal Complexes 2, 3, and 4 and its Parent Ligand 1 and Plot Exhibiting the Effect of Absorbance Measured Along with Various Doses of the Ligand and Metal Complexes Using the MTT Assay Method concerning Hela Cell Lines

Since all the complexes tested against different cell lines are more carcinogens than the parent ligand This demonstrates that the cytotoxicity of metal complexes is enhanced by the coordination of the DNA emulation by 1,10-phenanthroline substituted oxamides which is a known DNA intercalating aromatic planar ligand. Comparison of IC_{50} values of mononuclear metal complexes with both homo and hetero binuclear complexes in all the cell lines stands account for this. The IC_{50} values of mono and hetero bimetal metal complexes against selected cell lines are listed cell lines are tabulated in Table-6.

Table-6: MIC of Ligand and Metal Complexes Against Selected Cell Lines

Complex	Cancer cell lines		
	HeLA IC_{50} (μgmL^{-1})	HT-29 IC_{50} (μgmL^{-1})	A549 IC_{50} (μgmL^{-1})
1	69.05	62.69	-
2	32.15	-	-
3	37.43	32.45	70.23
4	34.36	35.16	73.47

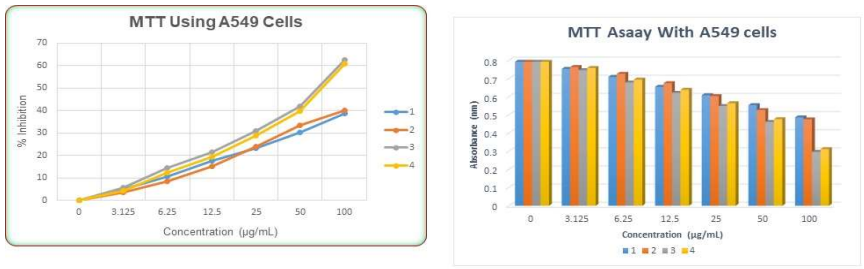

Fig.-30: Graphical Representation of Toxic Activity of Tested Metal Complexes Versus Different Concentration of Metal Complexes 2, 3, and 4 and its Parent Ligand 1 and Plot Exhibiting the Effect of Absorbance Measured Along with Various Doses of the Ligand and Metal Complexes Using the MTT Assay Method concerning A549 Cell Lines

Inhibition of Cell Cycle by Metal Complexes

Metal complexes actuate apoptosis against HeLa and HT29 cells. Complexes 2, 3, and 4 inhibit HeLa cells, and complexes 3 and 4 inhibit HT-29 cells which were further analyzed for apoptotic studies (Fig.-31-34).

Among the newly synthesized 2, 3, and 4 have shown prominent cytotoxic activity in HeLa cells, and complexes 3 and 4 have shown prominent cytotoxic activity in HT-29 cells. The percentage of cells gated are summarized in Table-7 and Table-8 for HeLa and HT29 cell lines respectively. Abnormal mutation of cells leads to cancer and these cells exhibit less population doubling time. A mature cell enters, G0/G1 phase which is the biggest phase in the cell cycle also it is the resting phase for the cell where the cell prepares all the necessary proteins for replication here DNA concentration will be 2n = 46 (23 pairs of chromosomes) After this DNA with 2n concentration enters synthesis phase (S phase) where DNA breaks down to single helical structure (with concentration 4n) and the next phase is G2M phase where karyokinesis or cytokinesis occurs and single-stranded DNA entirely becomes new cell by forming metaphase plate and two cells separate in opposite direction.[62] If the metal complex binds to DNA at this phase fluorescence can be observed in corners if the metal complex binds to DNA in the S phase then more fluorescence can be observed compared to that of the G0/G1 phase (since replication during the S phase raises the cell's DNA content from 2 to 4 nucleotides. HeLa cell lines treated with 25 µM and 50 µM of complex 2 have shown significant cell arrest at 19.80% and 28.5% in the S phase respectively and 8.56% and 10.66% in the G2M phase respectively, 25 µM and 50 µM of complex 3 treated with HeLa cell lines has gated 13.77% and 14.38% in S phase respectively and 8.27% and 12.51% in G2M phase respectively and also 25 µM and 50 µM of complex 4 treated with HeLa cell lines have gated 16.67% and 27.27% in S phase respectively and 12.59% and 7.85% in G2M phase respectively. With the increase in concentration, all three complexes have remarkably reduced viable cells in the resting phase (G0/G1) it can be concluded that complexes 2, 3, and 4 act as dose-dependent adducts for Hela cells. HT29 cells treated with 25 µM and 50 µM of complex 3 have shown significant cell arrest at 19.48% and 20.74% in the S phase respectively and 5.29% and 8.81% in the G2M phase respectively and 25 µM and 50 µM of complex 4 treated with HT29 cell lines has gated 20.73% and 22.68% in S phase respectively and 5.81% and 7.94% in G2M phase respectively. An increase in concentration of both bimetal oxamide complexes 3 and 4 has reduced viable cells significantly indicating that they can be used as dose-dependent anti-cancer drugs.

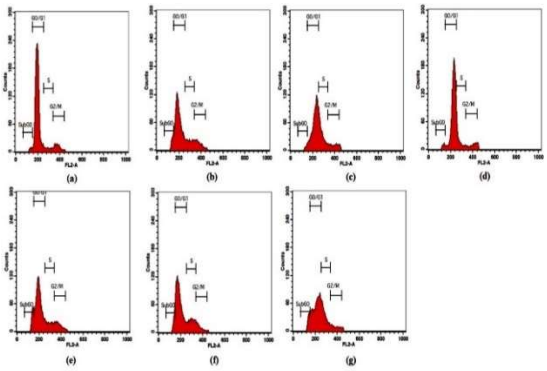

Fig.-31: Graphical Representation of Cell Cycle Distribution of HeLa Cells at 25 µM and 50 µM Metal Complex Concentrations, [2- (b) and (c) Respectively]; [3- (d) and (e) Respectively]; [4- (f) and (g) Respectively]; Whereas (a)-Control Plot Without Test Sample

Table-7: Cell Cycle Arrest in HeLa Cells by Metal Complexes 2, 3, and 4 by using FACS Analysis

		FACS cell cycle Studies of HeLa cell line			
	Conc. µM	G0	G0/G1	S	G2M
HeLa	Control	1.89	83.55	5.56	9.19
	(2) - 25 µM	9.5	64.18	19.8	8.56
	(2) - 50 µM	2.18	59.01	28.5	10.66
	(3) - 25 µM	2.72	74.85	13.77	8.27
	(3) - 50 µM	10.74	63.47	14.38	12.51
	(4) - 25 µM	6.96	65.08	16.67	12.59
	(4) - 50 µM	8.31	57.75	27.27	7.85

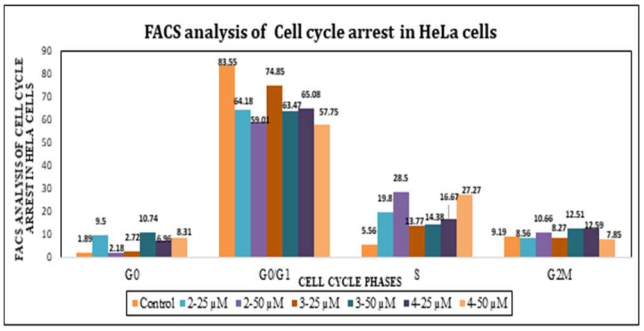

Fig.-32: Graphical Representation of Cell Cycle Arrest in HeLa Cells by Metal Complexes; 2, 3 and 4 at 25µM and 50 µM Concentration by using FACS Analysis

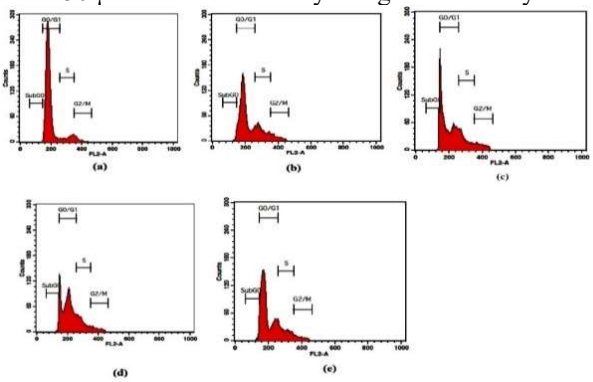

Fig.-33: Graphical Representation of Cell Cycle Distribution of HT-29 Cells Treated with; 25µM and 50 µM Metal Complex Concentrations, [3- (b) and (c) Respectively] and [4- (d) and (e) Respectively]; Whereas (a)-Control Plot Without Test Sample

Table-8: Cell Cycle Arrest in HT29 Cells by Metal Complexes 3 and 4 by FACS Analysis

		FACS cell cycle Studies of HT29 cell line			
	Conc. µM	G0	G0/G1	S	G2M
HT-29	Control	0.05	87.65	8.99	3.54
	3 - 25 µM	3.94	74.05	19.48	5.29
	3 - 50 µM	14.03	62.6	20.74	8.81
	4 - 25 µM	6.72	71.38	20.73	5.81
	4 - 50 µM	2.04	68.82	22.68	7.94

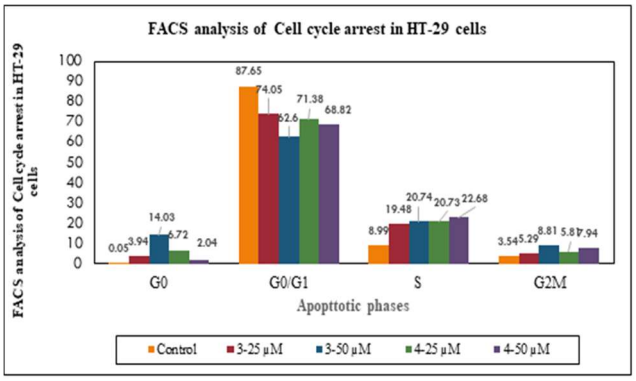

Fig.-34: Graphical Representation of Cell Cycle Arrest in HT29 Cells by Metal Complexes; 3 and 4 at 25µM and 50 µM Metal Complex Concentrations by using FACS Analysis.

Apoptosis of HeLa and HT-29 Cell Lines by Metal Complexes

It was found that newly synthesized complexes with 1,10-phenanthroline as terminal ligand utilizing ligand 1 actuate apoptosis against HeLa and HT29 cells. Complexes 2, 3, and 4 inhibit HT-29 cells (Fig.-35 to 38).

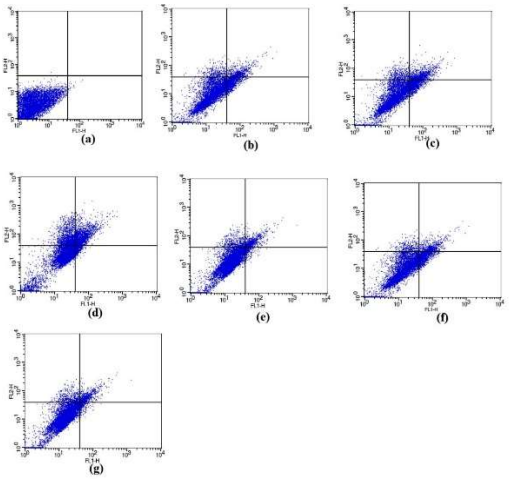

Fig.-35: Graphical Representation of Apoptotic Cell Distribution of HeLa Cells Treated with; at 25µM and 50 µM Metal Complex Concentrations, [2- (b) and (c) Respectively]; [3- (d) and (e) Respectively]; [4- (f) and (g) Respectively]; Whereas (a)-Control Plot Without Test Sample

Among the metal complexes analyzed for apoptosis against the HeLa cell line, bis-substituted cobalt mono metal complex 2, has shown 10.02%, 14.42% early apoptotic cells, and 0.33%, 10.92% late apoptotic cells, 0.23%, 4.49% necrotic cells at concentrations 25 µM, 50 µM respectively. Complex 3, has shown 3.46%, 5.06% early apoptotic cells and 8.16%, 19.24% late apoptotic cells, as 5.72%, 17.99% necrotic cells at concentrations 25 µM, and 50 µM respectively, and 13.63%, 4.06% early apoptotic cells, and 7.14%, 21.49% late apoptotic cells, also 3.36%, 19.33% necrotic cells at concentrations 25 µM, 50

µM were found respectively by the treatment of complex 4 (Table-9 and Table-10). Against HT29 cells, Complex 3, has shown 4.18%, 8.28% early apoptotic cells, and 17%, 18.28% late apoptotic cells, also 0.57%, 1.38% necrotic cells at concentrations 25 µM, and 50 µM respectively. Complex 4 has induced 1.59%, 10.90% early apoptotic cells and 20.11%, and 52.40% late apoptotic cells, respectively 1.94% and 0.67% necrotic cells were found compared to the control cells which did not show any cells gated in the same phase with respective cell lines. Metal complexes analyzed for apoptosis against the HeLa cell line with ligand 1 and N, N-donor heterocyclic base 1,10-phenanthroline has significantly arrested tumor cell growth in the late apoptotic phase. Bimetal complexes 3 and 4 at a higher dose (50 µM) have shown significant necrosis by 17.99 and 19.33% compared to a lower dose (25 µM) 5.72 and 3.36% from which it can be concluded that bi-metal cobalt complexes with heterocyclic base 1,10-phenanthroline are dose-dependent in activating programmed cell death.

Table-9: Apoptosis Detection in HeLa Cells by Metal Complexes 2, 3, and 4 by using Flow Cytometry Analysis

		FACS apoptosis Studies of HeLa cell line			
	Conc. µM	Viable cells	Early Apoptotic	Late Apoptotic	Necrotic cells
HeLa	Control	99.77	0.22	0	0.01
	2 - 25 µM	89.42	10.02	0.33	0.23
	2 - 50 µM	70.17	14.42	10.92	4.49
	3 - 25 µM	82.66	3.46	8.16	5.72
	3 - 50 µM	57.71	5.06	19.24	17.99
	4 - 25 µM	75.87	13.63	7.14	3.36
	4 - 50 µM	55.12	4.06	21.49	19.33

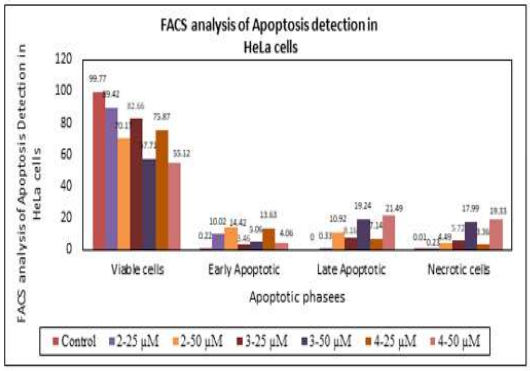

Fig.-36: Graphical Representation of Apoptosis Detection in HeLa Cells by Metal Complexes 3 and 4 at 25µM and 50 µM Metal Complex Concentrations by Using Flow Cytometry Analysis

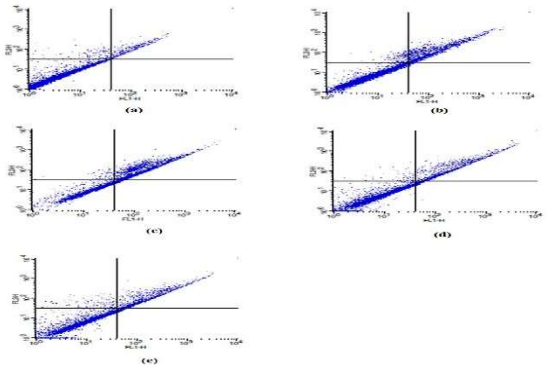

Fig.-37: Graphical Representation of Cell Apoptotic Cell Distribution of HT-29 cells 25 µM and 50 µM Metal Complex Concentrations Were used, [3- (d) and (e) Respectively]; [4- (f) and (g) Respectively]; Whereas (a)-Control Plot Without Test Sample

Table-10: Apoptosis Detection in HeLa Cells by Metal Complexes 3 and 4 by using Flow Cytometry Analysis

		FACS apoptosis Studies of HT29 cell line			
Cell line	Conc. µM	Viable cells	Early Apoptotic	Late Apoptotic	Necrotic cells
HT29	Control	93.83	0.03	4.8	1.34
	3-25 µM	78.25	4.18	17	0.57
	3-50 µM	72.06	8.28	18.28	1.38
	4-25 µM	76.36	1.59	20.11	1.94
	4-50 µM	36.03	10.9	52.4	0.67

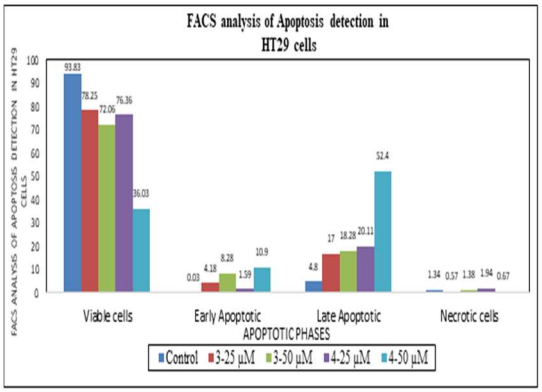

Fig.-38: Graphical Representation of Apoptosis Detection in HT29 Cells by Metal Complexes; 3 and 4 at 25µM and 50 µM Metal Complex Concentrations by Using Flow Cytometry Analysis

CONCLUSION

Binuclear metal complexes with varying metal centers of d-block and f-block metals exhibit enhanced abilities in antibacterial, antifungal, and antitumor activities and can be developed as dose-dependent antineoplastic drugs. Metal complexes with combinational metal centers augment the possible designing of therapeutic drugs targeting substrate molecules in a biological system which would be a future scope for medicinal chemistry and clinical pharmacology.

ACKNOWLEDGEMENTS

Swathi K. R., one of the authors, expresses her gratitude to the UGC for funding her RGNF fellowship so she could conduct this research. P R Chetana, a different author, acknowledges DST for providing her lab with a Gel-Documentation system.

CONFLICT OF INTERESTS

No conflicts of interest exist, according to the authors.

AUTHOR CONTRIBUTIONS

All the authors contributed significantly to this manuscript, participated in reviewing/editing and approved the final draft for publication. The research profile of the authors can be verified from their ORCID ids, given below:

K. R. Swathi http://orchid.org/0009-0006-4499-3907
M.N. Somashekar http://orchid.org/0000-0002-9882-2920
P. R. Chetana http://orchid.org/0000-0002-3331-07803

REFERENCES

1. M. Selvaganapathy and N. Raman, *Journal of Chemical Biology and Therapeutics,* **1(2)**, 108 (2016), https://doi.org/10.4172/2572-0406.1000108

2. C. K. Alexis, and K. B. Jacqueline, *Chemical Communications*, **49(35)**, 3617(2013), https://doi.org/10.1039/C3CC00177F
3. J. Benjamin, D. L. Ang, E. P. Wright, Aldrich-Wright and R. Janice, *Dalton Transactions*, **44(8)**, 3505(2015), https://doi.org/10.1039/C4DT02700K
4. P. Zhang and J. P. Sadler, *European Journal of Inorganic Chemistry*, **2017(12)**, 1541(2017), https://doi.org/10.1002/ejic.201600908
5. G. Mahanthesha, T. Suresh and T. R. Ravikumar Naik, *Rasayan Journal of Chemistry*, **15(1)**, 155(2022), http://dx.doi.org/10.31788/RJC.2022.1516577
6. D. S. Sigman, A. Mazumder and D. M. Perrin, *Chemical Reviews*, **93**, 2295(l993),https://doi.org/10.1021/cr00022a011
7. Li Xiang, Yuhui Wang, Li Man, Huipeng Wang and Xiongwei Dong, *Molecules*, **27(1)**, 148(2021), https://doi.org/10.3390/molecules27010148
8. Yan-Tuan Li, Qiang-Ming Wu, Cui-Wei Yan and Chun-Yuan Zhu, *Journal of Magnetism and Magnetic Materials*, **283(2-3)**, 215(2004), https://doi.org/10.1016/j.jmmm.2004.05.025
9. P. R. Chetana, R. Rao, Debojyoti Lahiri, R.S. Policegoudra, S. Ravish, and M.S. Aradhya, *Polyhedron*, **68**, 172(2014), https://doi.org/10.1016/j.poly.2013.10.025
10. Lay Xiao-Wen, Man Jiangy, Li Yan-Tuan, Zhi-Yong Wuy and Cui-Wei Yan, *Journal of Coordination Chemistry,* **63(10)**, 1582(2010), https://doi.org/10.1080/00958972.2013.827179
11. Wen-Cai Chen, Ling-Dong Wang, Li Yan-Tuan, Wu Zhi-Yong and Yan Cui-Wei, *Transition Metal Chemistry,* **37**, 569(2012), https://doi.org/10.1007/s11243-012-9623-2
12. L. Ningjian and D. K. David, *Molecules,* **19**, 19180(2014), https://doi.org/10.3390/molecules191119180
13. Y. Sumanont, Y. Murakami, M. Tohda, O. Vajragupta, K. Matsumoto and H. Watanabe, *Biological and Pharmaceutical Bulletin*, **27(2)**, 170(2004), https://doi.org/10.1248/bpb.27.170
14. Z. Xiu-Mei, T. Jie, W. Li-Na, Y. Di, Y. Qing, H. Fu-Ping, B. He-Dong, *Polyhedron*, **133(5)**, 433(2017), https://doi.org/10.1016/j.poly.2017.05.026
15. R.J. Gonzalez and J.B. Tarloff, *Toxicology in Vitro*, **15**, 257(2001), https://doi.org/10.1016/s08872333(01)00014-5
16. A. Lundin, M. Hasenson, J. Pearson and A. Pousette, *Methods in Enzymology,* **133**, 27(1983), https://doi.org/10.1016/0076-6879(86)33053-2
17. F. Denizot and R. Lang, *Journal of Immunological Methods*, **89**, 271(1986), https://doi.org/10.1016/0022-1759(86)90368-6
18. H. Jahangirian, Md Jelas Haron, Mohd. H. S. Ismail, R. Rafiee-Moghaddam, L. Afsah-Hejri, Y. Abdollahi, M. Rezayi and N. Vafaei, *Digest Journal of Nanomaterials and Biostructures,* **8(3)**, 1263(2013)
19. T. Ahamad, V. Kumar, S. Parveen and N. Nishat, *Journal of Coordination Chemistry*, **61(9)**, 1423(2008), https://doi.org/10.1080/00958970701579290
20. Jia-qing Xie, Bing-ying Jiang, Xing-ming Kou, Chang-wei Hu and Xian-cheng Zeng, *Transition Metal Chemistry*, **28**, 782(2003), https://doi.org/10.1023/A:1026014625203
21. Fang-Hong He, Lin Tao, Li Xiao-Wen, Yan-Tuan, Zhi-Yong Wub and Cui-Wei Yan, *New Journal of Chemistry*, **36**, 2078(2012), https://doi.org/10.1039/C2NJ40397H
22. J. Jackman, and P.M.O. Connor, *Current Protocols in Cell Biology*, (2001), https://doi.org/10.1002/0471143030.cb0803s00
23. 23 A. Z. Vajihe, G. Hossein and E. Janzamin, *Indian Journal of Pharmacology,* **44(6)**, 714(2012), https://doi.org/10.4103/0253-7613.103265
24. P. T. Ramesh, S. Subramanian, E. M. Campbell, V. Rangasamy, T. Nithyananda, G. Sondarva, S. Mehrotra, P. Mishra, Erin Zook, P. T. Le, A. Rana and B. Rana, *Journal of Biological Chemistry,* **286(43),** 37470(2011), https://doi.org/10.1074/jbc.M111.298943
25. E. Brauchle, S. Thude, Y. S. Brucker and S.L. Katja, *Scientific Reports,* **4**, 4698(2014). https://doi.org/10.1038/srep04698
26. K. J. Madhuravasal, V. Jaichandran, H. N. R. Madhavan, L. Vijaya, R. J. George, P. S. Ambastha, A. Manu and J. Malathi, *Biomedical Hub*, **3**, 1(2018), https://doi.org/10.1159/000491074

27. C. H. Homburg, M. De Haas, A. E. von dem Borne, A. J. Verhoeven, C. P. Reutelingsperger and D. Roos, *Blood,* **85(2)**, 532(1995)
28. G. Koopman, C. P. Reutelingsperger, G. A. Kuijten, R. M. Keehnen, S. T. Pals and M. H. van Oers, *Blood,* **84(5)**, 1415(1994)
29. C. Rebecca, Taylor, S. P. Cullen and S.J. Martin, *Molecular Cell Biology*, **9(3)**, 231(2008), https://doi.org/10.1038/nrm2312
30. S. J. Martin, C. P. Reutelingsperger, A. J. McGahon, J. A. Rader, R. C. Van Schie, D. M. LaFace and D. R. Green, *Journal of Experimental Medicine,* **182(5)**, 1545(1995), https://doi.org/10.1084/jem.182.5.1545
31. M. Van Engeland, F. C. Ramaekers, B. Schutte and C. P. M. Reutelingsperger, *Cytometry,* **24**, 131(1996), https://doi.org/10.1002/(SICI)1097-0320(19960601)24:2<131::AID-CYTO5>3.0.CO;2-M
32. I. Vermes, C. Haanen, H. Steffens-Nakken and C. Reutelingsperger, *Journal of Immunological Methods,* **184**, 39(1995), https://doi.org/10.1016/0022-1759(95)00072-i
33. M. Shimaoka, T. Iida, A. Ohara, N. Taenaka, T. Mashimo, T. Honda and I. Yoshiya. *Biochemical and Biophysical Research Communications*, **209(2)**, 519(1995), https://doi.org/10.1006/bbrc.1995.1532
34. K. Ajaykumar, S. A. Patil and P. S. Badami, *European Journal of Medicinal Chemistry*, **44**, 2904(2009), https://doi.org/10.1016/j.ejmech.2008.12.012
35. Li Xiao-Wen, Li Yan-Tuan, Wu Zhi-Yong, Y. Cui-Wei, *Inorganica Chimica Acta*, **390**, 190(2012), https://doi.org/10.1016/j.ica.2012.04.032
36. Li Yan-Tuan, Y. Cui-Wei, Zhu Chun-Yuan and Guan Hua-Shi, *Synthesis and Reactivity in Inorganic and Metal-Organic Chemistry*, **34**, 1165(2004), https://doi.org/10.1081/SIM-120039264
37. K. Siddappa, S. B. Mane and D. Manikprabhu, *Spectrochimica Acta, Molecular and Biomolecular Spectroscopy*, **130**, 634(2014), https://doi.org/10.1016/j.saa.2014.03.115
38. Lin-Lin Zhang, Ling-Dong Wang, Shu-Hui Zhan, Li Yan-Tuan, Wu Zhi-Yong and Y. Cui-Wei, *Structural Chemistry,* **25**, 103(2014), https://doi.org/10.1007/s11224-013-0255-8
39. Yu-Lan Song, Yan-Tuan Li and Zhi-Yong Wu, *Journal Inorganic Biochemistry,* **102**, 1691(2008), https://doi.org/10.1016/j.jinorgbio.2008.04.005
40. Li Yan-Tuan, Yan Cui-Wei, Lou Jian-Fang and Guan Hua-Shi, *Journal of Magnetism and Magnetic Materials,* **281**, 68(2004), https://doi.org/10.1016/j.jmmm.2004.03.049
41. U. Casellato, P. Guerriero, S. Tamburini and P. A. Vigato. *Inorganica Chimica Acta,* **260**, 1(1997), https://doi.org/10.1016/S0020-1693(96)05520-X
42. R. F. Beeston, S. Aldridge, J. Treadway, M. Fitzgerald, B. DeGraff, and S. Stitze, *Inorganic Chemistry*, **37**, 4368(1998), https://doi.org/10.1021/ic971322f
43. P. R. Chetana, R. Rao, S. Saha,. R. S. Policegoudra, P. Vijayan and M. S. Aradhya, *Polyhedron,* 43(2012), https://doi.org/10.1016/j.poly.2012.08.081
44. D. M. Boghaei and M. Gharagozlou, *Spectrochimica Acta*, Part A, **67**, 944(2007), https://doi.org/10.1016/j.saa.2006.09.012
45. Yan-Tuan Li, Chun-Yuan Zhu, Guo-Qiang Li, Cui-Wei Yan and Gui-Yun Xu, *Transition Metal Chemistry,* **30**, 850(2005), https://doi.org/10.1007/s11243-005-6206-5
46. Cui-Wei Yan, Yan-Tuan Li and Dai-Zheng Liao, *Transition Metal Chemistry,* **22**, 475(1997), https://doi.org/10.1023/A:1018559229011
47. E. M. Mrkalic, R. M. Jelic, O. R. Klisuric and Z. D. Matovic, *Dalton Transactions*, **43**, 15126(2014), https://doi.org/10.1039/C3DT53384K
48. A. Steckel and G. Schlosser, *Molecules,* **24(3)**, 611(2019), https://doi.org/10.3390/molecules24030611
49. L. Konermann, E. Ahadi, A. D. Rodriguez and S. Vahidi, *Analytical Chemistry*, **85**, 2(2013), https://doi.org/10.1021/ac302789c
50. H. Paul, R. Chakraborty, P. Chattopadhyay, *Rasayan Journal of Chemistry,* **15(1)**, 452(2022), http://dx.doi.org/10.31788/RJC.2022.1516706
51. Wen-Cai Chen, Ling-Dong Wang, Yan-Tuan Li, Zhi-Yong Wu and Cui-Wei Yan, *Transition Metal Chemistry*, **37**, 569(2012), https://doi.org/10.1007/s11243-012-9623-2

52. Tian-Rong Li, Zheng Yin Yang, Bao-Dui Wang, Dong-Dong Quin, *European Journal of Medicinal Chemistry,* **43**, 1688(2008), https://doi.org/10.1016/j.ejmech.2007.10.006
53. L. H. Abdel-Rahman, R. M. El-Khatib, L. A. E. Nassr, A. M. Abu-Dief, Mohamed Ismael and A. A. Seleem, *Spectrochimica Acta A Molecular and Biomolecular Spectroscopy,* **117**, 366(2014), https://doi.org/10.1016/j.saa.2013.07.056
54. N. Ramana, S. Sobha, A. Thamaraichelvan, *Spectrochimica Acta A Molecular and Biomolecular Spectroscopy*, **78**, 888(2011), https://doi.org/10.1016/j.saa.2010.12.056
55. A. M. Dar, U. Ishrat, Z. Yaseen, Shamsuzzaman and M.A. Gatoo, *Journal of Photochemistry and Photobiology B: Biology* **148**, 340(2015), https://doi.org/10.1016/j.jphotobiol.2015.04.031
56. A. C. Ekennia, A. A. Osowole, L. O. Olasunkanmi, D. Onwudiwe, E. Ebenso, *Research on Chemical Intermediates*, **43(7)**, 3787(2017), https://doi.org/10.1007/s11164-016-2841-z
57. N. Nishat, M. Rahisuddin, M. M. Haq and Vikrant Kumar, *Journal of Coordination Chemistry*, **59(15)**, 1729(2006), https://doi.org/10.1080/00958970600611673
58. K. P. Panchal, H. M. Parekh, P. B. Pansuriya and M.N. Patel, *Journal of Enzyme Inhibition and Medicinal Chemistry,* **21(2)**, 203(2006), https://doi.org/10.1080/14756360500535229
59. A. F. Santosa, D. F. Brottoa, L. R. V. Favarina, N. A. Cabezaa, G. R. Andradea, M. Batistotea, A. A. Cavalheiroa, A. Nevesb, C. M. Rodriguesa and A.D. Anjosa, *Revista Brasileira de Farmacognosia,* **24(3)**, 309(2014), https://doi.org/10.1016/j.bjp.2014.07.008
60. A. A. Thebo, N. A. Nahyoon, S. N. Phulpoto, Azim Khan, S. A. Shah, Sajjad Ali and K. H. Thebo, *Organic and Medicinal Chemistry International Journal,* **2(1)**, 1(2017), https://doi.org/10.19080/OMCIJ.2017.02.555578
61. Raj Kaushal, Sheetal Thakur and Kiran Nehra, *International Journal of Medicinal Chemistry*, 2361214, 11(2016), https://doi.org/10.1155/2016/2361214
62. Gerald Litwack, *Vitamins and Harmones: Cell Death Proteins,* Vol. 52, (1996).

[RJC-8501/2023]